Monthly Notices of the ROYAL ASTRONOMICAL SOCIETY

MNRAS **513,** 5666–5685 (2022)
Advance Access publication 2022 May 6

https://doi.org/10.1093/mnras/stac1228

Progenitor, environment, and modelling of the interacting transient AT 2016jbu (Gaia16cfr)

S. J. Brennan [1★] M. Fraser [1★] J. Johansson [2★] A. Pastorello [3] R. Kotak,[4] H. F. Stevance [5] T. -W. Chen [6,7] J. J. Eldridge [5] S. Bose [8,9] P. J. Brown [10] E. Callis [1] R. Cartier,[11] M. Dennefeld,[12] Subo Dong,[13] P. Duffy,[1] N. Elias-Rosa [3,14] G. Hosseinzadeh [15] E. Hsiao [16] H. Kuncarayakti,[17,18] A. Martin-Carrillo,[1] B. Monard,[19] G. Pignata [20,21] D. Sand [22] B. J. Shappee [23] S. J. Smartt,[24] B. E. Tucker [25,26,27] L. Wyrzykowski [28] H. Abbot,[25] S. Benetti [3] J. Bento [25] S. Blondin [29,30] Ping Chen,[27] A. Delgado,[31,32] L. Galbany [14] M. Gromadzki [28] C. P. Gutiérrez [17,18] L. Hanlon,[1] D. L. Harrison [31,33] D. Hiramatsu [34,35,36,37] S. T. Hodgkin [31] T. W.-S. Holoien [38] D. A. Howell [34,35] C. Inserra [39] E. Kankare [4] S. Kozłowski [28] T. E. Müller-Bravo [14,40] K. Maguire [41] C. McCully [34,35] P. Meintjes,[42] N. Morrell [43] M. Nicholl,[44,45] D. O'Neill,[24] P. Pietrukowicz [28] R. Poleski [28] J. L. Prieto,[21,46] A. Rau,[7] D. E. Reichart [47] T. Schweyer,[6,7] M. Shahbandeh,[48] J. Skowron [28] J. Sollerman [6] I. Soszyński [28] M. D. Stritzinger [49] M. Szymański [28] L. Tartaglia [3] A. Udalski [28] K. Ulaczyk [28,50] D. R. Young [51] M. van Leeuwen[31] and B. van Soelen [42]

Affiliations are listed at the end of the paper

Accepted 2022 April 27. Received 2022 April 27; in original form 2021 February 16

ABSTRACT

We present the bolometric light curve, identification and analysis of the progenitor candidate, and preliminary modelling of AT 2016jbu (Gaia16cfr). We find a progenitor consistent with a $\sim$ 22–25 $M_\odot$ yellow hypergiant surrounded by a dusty circumstellar shell, in agreement with what has been previously reported. We see evidence for significant photometric variability in the progenitor, as well as strong Hα emission consistent with pre-existing circumstellar material. The age of the environment, as well as the resolved stellar population surrounding AT 2016jbu, supports a progenitor age of >10 Myr, consistent with a progenitor mass of $\sim$22 $M_\odot$. A joint analysis of the velocity evolution of AT 2016jbu and the photospheric radius inferred from the bolometric light curve shows the transient is consistent with two successive outbursts/explosions. The first outburst ejected material with velocity $\sim$650 km s^{-1}, while the second, more energetic event ejected material at $\sim$4500 km s^{-1}. Whether the latter is the core collapse of the progenitor remains uncertain. We place a limit on the ejected ^{56}Ni mass of <0.016 $M_\odot$. Using the Binary Population And Spectral Synthesis (BPASS) code, we explore a wide range of possible progenitor systems and find that the majority of these are in binaries, some of which are undergoing mass transfer or common-envelope evolution immediately prior to explosion. Finally, we use the SuperNova Explosion Code (SNEC) to demonstrate that the low-energy explosions within some of these binary systems, together with sufficient circumstellar material, can reproduce the overall morphology of the light curve of AT 2016jbu.

Key words: stars: massive – supernovae: general – supernovae: individual: AT 2016jbu.

1 INTRODUCTION

This is the second of two works on the interacting transient AT 2016jbu (Gaia16cfr). We report photometric and spectroscopic observations in Brennan et al. (2021, hereafter Paper I) and present an in-depth comparison of AT 2016jbu and SN 2009ip-like transients, which include SN 2009ip (Fraser et al. 2013a; Graham et al. 2014), SN 2015bh (Elias-Rosa et al. 2016; Thöne et al. 2017), LSQ13zm (Tartaglia et al. 2016a), SN 2013gc (Reguitti et al. 2019), and SN 2016bdu (Pastorello et al. 2018). The work presented here will focus on the progenitor candidate and its environment, as well as modelling and interpretation of the spectral and photometric evolution.

AT 2016jbu shows a smooth evolution of the Hα emission profile, changing from a P Cygni profile, typically seen in Type II supernova (SN) spectra, which show strong, singular peaked hydrogen emission lines (Kiewe et al. 2012; Taddia et al. 2015), to a double-peaked emission profile that persists until late times, indicating complex, H-rich circumstellar material (CSM). AT 2016jbu and SN

★ E-mail: sean.brennan2@ucdconnect.ie (SJB); joeljo@fysik.su.se (JJ); morgan.fraser@ucd.ie (MF)

© 2022 The Author(s)
Published by Oxford University Press on behalf of Royal Astronomical Society

Downloaded from https://academic.oup.com/mnras/article/513/4/5666/6581584 by University of Arizona user on 02 September 2022

2009ip-like objects show strong similarities in late-time spectra, with strong Ca II, He I, and H emission lines as well as a lack of any emission from explosively nucleosynthesized material such as [O I] λλ 6300, 6364 or Mg I] λ4571. No clear nebular phase is seen even ∼ 1.5 years after explosion in AT 2016jbu, and ongoing interaction with CSM at late times may be hiding a nebular phase and/or inner material from the progenitor.

The nature of SN 2009ip-like transients is much more contentious. On one hand, there is evidence that these are genuine core-collapse supernovae (CCSNe): the progenitor was destroyed and the transient will fade after CSM interaction finishes (Smith & Mauerhan 2012; Pastorello et al. 2013, 2019a; Graham et al. 2014; Smith, Mauerhan & Prieto 2014). On the other hand, some suggest that these may be non-terminal events (Fraser et al. 2013a, 2015; Margutti et al. 2014; Graham et al. 2017) and SN 2009ip-like events are a result of either pulsational-pair instabilities (Woosley, Blinnikov & Heger 2007; Marchant et al. 2019), binary interaction (Kashi, Soker & Moskovitz 2013; Pastorello et al. 2019a), merging of massive stars (Soker & Kashi 2013), or instabilities associated with rapid rotation close to the ΩΓ limit (Maeder & Meynet 2000).

As a follow-up to Paper I, we continue the discussion on AT 2016jbu, focusing on the progenitor and its local environment, as well as examining the controversial topic of the powering mechanism behind SN 2009ip-like events. We note that some of these topics have been discussed before by Kilpatrick et al. (2018, hereafter referred to as K18) and we refer to this work throughout. For consistency with Paper I and for comparison with the previous work by K18, we take the distance modulus for NGC 2442 to be 31.60 ± 0.06 mag. This corresponds to a distance of 20.9 ± 0.58 Mpc and we adopt a redshift $z = 0.00489$ from the H I Parkes All-Sky Survey (HIPASS: Wong et al. 2006). The foreground extinction towards NGC 2442 is taken to be $A_V = 0.556$ mag (Schlafly & Finkbeiner 2011) via the NASA Extragalactic Database (NED[1]). We correct for foreground extinction using $R_V = 3.1$ and the extinction law given by Cardelli, Clayton & Mathis (1989). We do not correct for any host galaxy or circumstellar extinction; however, note that the blue colours seen in the spectra of AT 2016jbu do not point towards significant reddening by additional dust (discussed further in Section 4.2 and Section 2). We take the *V*-band maximum at *Event B* (as determined through a polynomial fit) as our reference epoch (MJD 57784.4 ± 0.5; 2017 January 30). Significant light-curve features will use the same naming convention as in Paper I for specific points in the light curve: *Rise, Decline, Plateau, Knee, Ankle*.

In Section 5 we investigate the CSM environment around AT 2016jbu and, using photometry presented in Paper I, reconstruct the bolometric evolution of *Event A* and *Event B* up until the seasonal gap (+140 days), which we discuss in Section 5.1. The progenitor of AT 2016jbu is discussed in Section 2 using pre-explosion as well as late-time imaging from the *Hubble Space Telescope* (*HST*). This presence of pre-existing dust is discussed in AT 2016jbu using Spectral Energy Distribution (SED) fitting as well as DUSTY modelling in Section 3. Using *HST* and Very Large Telescope (VLT) + Multi Unit Spectroscopic Explorer (MUSE) observations, we investigate the surrounding stellar population and environment in Section 4. The powering mechanism behind AT 2016jbu is discussed in Section 6. In Section 7.1, the most likely progenitor for AT 2016jbu is examined. AT 2016jbu and most SN 2009ip-like transients display a high degree of asymmetry, most likely due to a complex CSM environment, and this is expanded upon in Section 7.2. Finally, we will address the explosion scenario for AT 2016jbu and perhaps other SN 2009ip-like transients, focusing on a CCSN scenario in Section 7.4 and an explosion in a binary system in Section 7.5.

2 THE PROGENITOR OF AT 2016JBU

The progenitor of AT 2016jbu was discussed by K18, who suggest that it is consistent with an F8-type star of ∼18 $M_\odot$ from an optical SED fit, although circumstellar extinction places this as a lower bound.

There is a wealth of pre-explosion images of NGC 2442 and in this section we explore these data to identify and characterize the progenitor of AT 2016jbu. Here we are concerned specifically with the quiescent (or apparently quiescent) progenitor, which can only be identified in deep, high-resolution data.

2.1 *Hubble Space Telescope* imaging of the progenitor

NGC 2442 was observed with the *HST* on a number of occasions both prior to and after the discovery of AT 2016jbu using the Advanced Camera for Surveys (ACS) and both the UV–visible and IR channels of the Wide-Field Camera 3 (WFC3/UVIS and WFC3/IR). We retrieved all images where the image footprint covered the site of AT 2016jbu from the Mikulski Archive for Space Telescopes (MAST[2]); these data are listed in Table 1. In all cases, science-ready reduced images were downloaded. With the exception of the late-time ACS images taken in 2019, all analysis was performed on frames that have already been corrected for charge-transfer efficiency losses at the pixel level (i.e. DRC/FLC files). For the 2019 ACS images, corrections for charge-transfer efficiency were applied to the measured photometry.

In order to locate a progenitor candidate for AT 2016jbu, we aligned the *F814W*-filter image taken in 2017, when the transient was bright, with the ACS + *F814W* image from 2006, approximately ten years prior to discovery. Using 20 point sources common to both frames and within 20 arcsec of AT 2016jbu, we derive a transformation between the pixel coordinates with a root-mean-square (rms) scatter of only 12 milliarcseconds (mas; pixel scale ∼ 0.05 arcsec pixel^{-1}). A bright source is clearly visible at the position, and we identify this as the progenitor candidate. The progenitor candidate is shown in Fig. 1 and is the same source as was identified by K18.

We performed point-spread photometry (PSF) fitting on all *HST* images using the 2019 November release of the DOLPHOT package (Dolphin 2000), with the instrument-specific ACS and WFC3 modules. In all cases, we performed photometry following the instrument-specific recommendations of the DOLPHOT handbook[3] regarding choice of aperture size. The WFC3 images were taken at two distinct pointings, and each set was analysed separately, otherwise each contiguous set of imaging with a particular instrument was photometered together, using a single deep drizzled image as a reference frame for source detection. Examination of the residual images after fitting and subtracting a PSF for sources in the field revealed no systematic residuals, indicating satisfactory fits in all cases. We show the *HST* photometry for AT 2016jbu in Fig. 2.

We find that the photometry reported by K18 is fainter than we measure, with a difference of ∼0.5 mag in *F350LP*. We compared our measured *F350LP* magnitudes and those of K18 with the values

[1] https://ned.ipac.caltech.edu/

[2] mastweb.stsci.edu/

[3] http://americano.dolphinsim.com/dolphot/dolphot.pdf

Downloaded from https://academic.oup.com/mnras/article/513/4/5666/6581584 by University of Arizona user on 02 September 2022

Table 1. Observational log for all *HST* images covering the site of AT 2016jbu. Measured photometry (in the Vega mag system) for AT 2016jbu is also reported. Phase is in rest-frame days relative to *Event B* maximum light (MJD 57784.4).

Date	Phase (d)	Instrument	Filter	Exposure (s)	Mag (err)
2006-10-20	−3736.0	ACS/WFC	F435W	4 × 395	24.999 (0.037)
–	–	–	F658N	3 × 450	21.207 (0.024)
–	–	–	F814W	3 × 400	23.447 (0.019)
2016-01-21	−373.1	WFC3/UVIS	F350LP	1 × 420	23.625 (0.017)
–	–	WFC3/IR	F160W	2 × 503	20.726 (0.003)
2016-01-31	−362.9	WFC3/UVIS	F350LP	2 × 420	22.215 (0.026)
–	–	–	F555W	2 × 488	22.645 (0.002)
2016-02-08	−354.4	WFC3/UVIS	F350LP	3 × 420	22.134 (0.001)
–	–	WFC3/IR	F160W	2 × 503	19.570 (0.005)
2016-02-17	−345.5	WFC3/UVIS	F350LP	3 × 420	23.108 (0.012)
–	–	–	F814W	2 × 488	22.287 (0.003)
2016-02-23	−339.9	WFC3/UVIS	F350LP	3 × 420	23.212 (0.022)
2016-02-28	−334.8	WFC3/UVIS	F350LP	1 × 420	23.985 (0.022)
–	–	–	F555W	2 × 488	24.399 (0.004)
2016-03-04	−330.4	WFC3/UVIS	F350LP	3 × 420	22.729 (0.022)
–	–	WFC3/IR	F160W	2 × 503	20.224 (0.011)
2016-03-10	−323.8	WFC3/UVIS	F350LP	3 × 420	22.690 (0.037)
–	–	–	F814W	2 × 488	21.967 (0.022)
2016-03-15	−318.8	WFC3/UVIS	F350LP	3 × 420	22.868 (0.016)
–	–	WFC3/IR	F160W	2 × 503	20.323 (0.014)
2016-03-21	−313.1	WFC3/UVIS	F350LP	3 × 420	23.400 (0.013)
–	–	–	F555W	2 × 488	23.962 (0.012)
2016-03-30	−304.2	WFC3/UVIS	F350LP	3 × 420	23.775 (0.006)
–	–	WFC3/IR	F160W	2 × 503	21.301 (0.020)
2016-04-09	−293.7	WFC3/UVIS	F350LP	3 × 420	23.767 (0.006)
–	–	–	F814W	1 × 488	23.079 (0.035)
2019-03-21	+ 776.7	WFC3/UVIS1	F555W	320,390	23.882 (0.025)
–	–	–	F814W	2 × 390	23.239 (0.032)
2019-03-31	+ 787.0	ACS/WFC	F814W	4 × 614	23.529 (0.014)

reported in the Hubble Source Catalog (HSC: Whitmore et al. 2016). As the magnitudes reported in the HSC are in the AB mag system, we applied the conversion from AB to Vega mag before comparing them with our photometry. The HSC *F350LP* magnitudes are consistent with those we report here and we also see the same variability for the progenitor candidate. The cause of the difference between our photometry and that of K18 hence remains unknown.

We note that the broad-band photometry from *HST* is more than likely affected by the strong emission in Hα. In Fig. 3 we show the throughput of the *HST* filters compared with a late-phase spectrum of AT 2016jbu. The long-pass *F350LP* filter will contain flux from Hα. Fortuitously, Hα falls in the low-throughput red wing of the *F555W* filter, where it will have negligible effect. To verify this, we used SYNPHOT (Lim 2020) to perform synthetic *F555W*-filter photometry on the +271 d spectrum of AT 2016jbu and on the same spectrum where Hα has been excised. The latter returns a magnitude that is only 0.05 mag fainter than the former, and so the *F555W* filter is not affected significantly by line emission.

The progenitor is relatively red, bright, and shows significant variability over time-scales of ∼weeks. Correcting for foreground extinction, in 2006 the progenitor candidate had an absolute magnitude in $F814W = -8.46 \pm 0.06$ and an $F435W - F814W$ colour of 1.13 ± 0.04 mag. This colour is consistent with a yellow hypergiant (YHG) and corresponds to a blackbody temperature of 6500 K (Drilling & Landolt 2000).

However, the narrow-band *F658N* magnitude, which covers Hα, is much brighter than would be expected. This indicates that even ten years before the eruption or explosion of AT 2016jbu its progenitor was characterized by strong Hα emission.

In early 2016, between seven and ten months prior to the start of *Event A*, NGC 2442 was observed repeatedly with WFC3 in *F350LP*, *F555W*, *F814W*, and *F160W*. This dataset gives us a unique insight into the variability of the quiescent progenitor prior to explosion. We see that even in quiescence (arbitrarily defined as when the progenitor is fainter than mag ∼−10), the progenitor displays strong variability. In particular, in the best-sampled *F350LP* light curve the progenitor varies in brightness by 1.9 mag in only 20 days. As discussed by K18, such rapid variability is hard to explain (although there is some similarity to the fast variability seen in the pre-explosion light curve of SN 2009ip: Pastorello et al. 2013). While it is impossible to know if the variability is periodic on the basis of the short time coverage available for AT 2016jbu, if it is periodic then the apparent period is around 45 days (found via a low-order polynomial fit to the *F350LP* light curve).

The variability seen in *F350LP* in early 2016 is also seen in other bands, which appear to track the same overall pattern of brightening and fading. Fig. 2 shows the colour evolution of *F350LP-F555W*, *F350LP-F814W*, and *F350LP-F160W*. In all cases (with the exception of the earliest *F350LP-F160W* colour, which is likely due to a spurious *F350LP* magnitude), we see a relatively minor colour change over three months. In fact, it is possible that the apparent small shift towards bluer colours is simply due to Hα growing stronger, which would cause the *F350LP* magnitude to appear brighter, rather than any change in the continuum temperature.

Downloaded from https://academic.oup.com/mnras/article/513/4/5666/6581584 by University of Arizona user on 02 September 2022

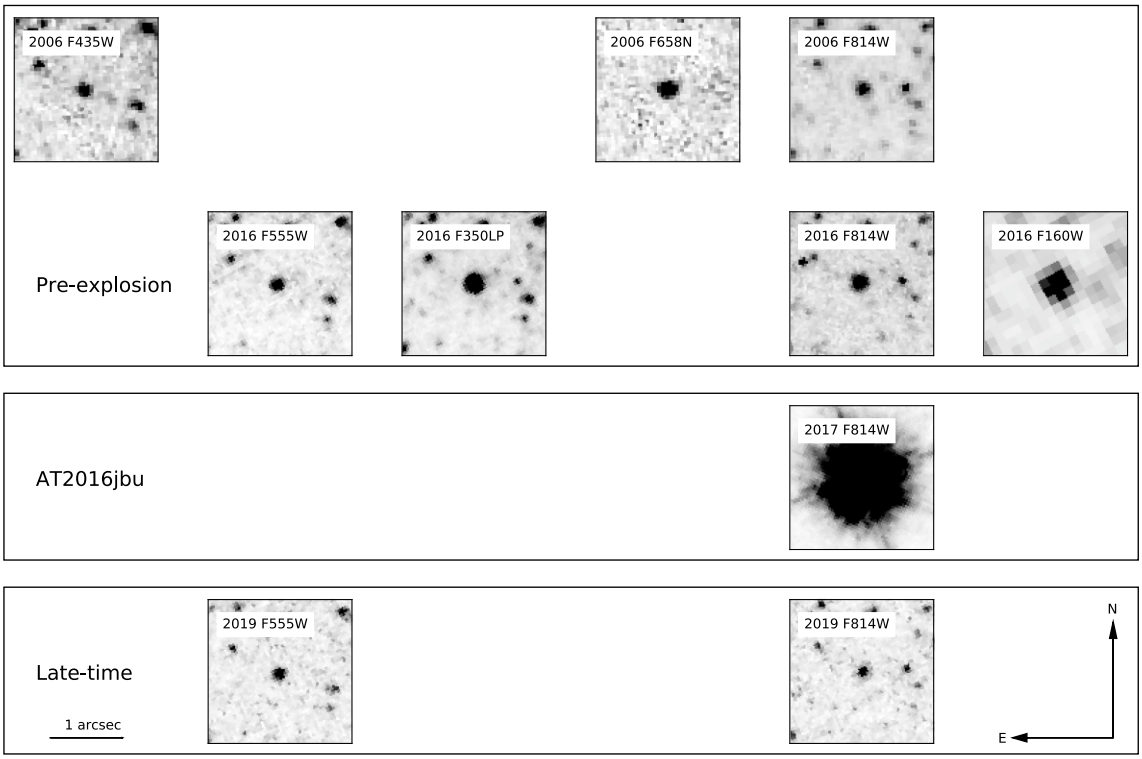

Figure 1. 2×2 arcsec^2 cutouts of all *HST* images centred on the progenitor candidate for AT 2016jbu. Columns are ordered in wavelength from left to right.

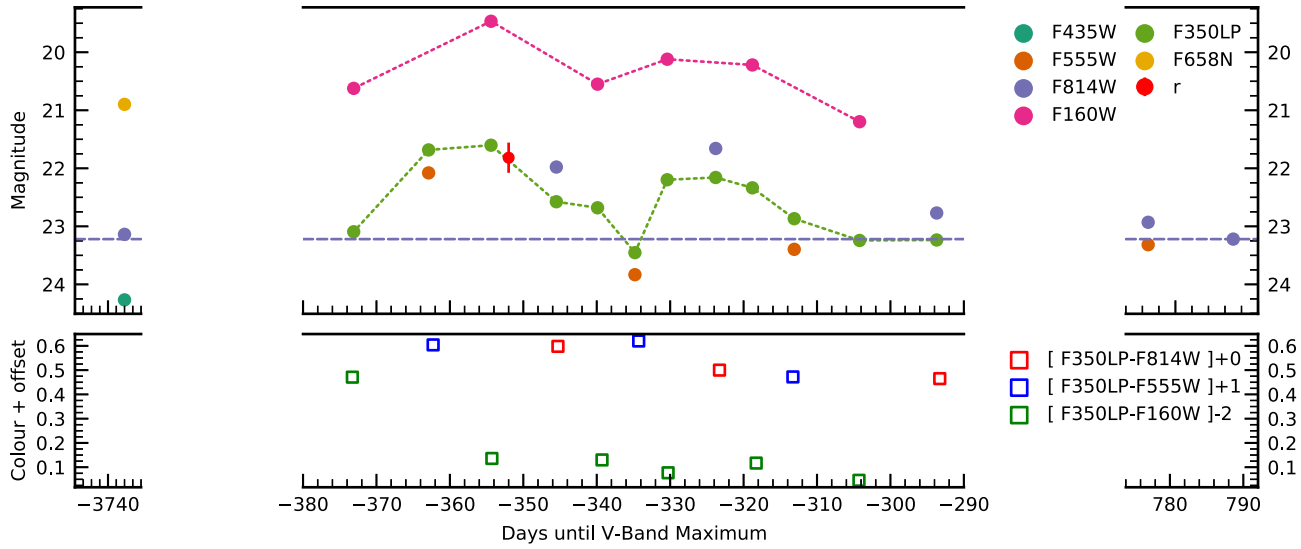

Figure 2. Foreground-extinction-corrected *HST* light curves of AT 2016jbu and its progenitor are shown in the top panel. We also include a DECam *r*-band detection at −352 d as a red filled circle with error bars. Error bars for *HST* measurements are smaller than the point sizes. The horizontal line is to guide the eye in comparing the late-time (∼+2 year) and pre-outburst (∼−10 year) *F814W* magnitudes. We also plot the *F350LP* and *F160W* light curves with a line to help guide the eye. Colour curves, corrected for foreground reddening, are shown in the bottom panel. Colours are offset for legibility by the amounts stated in the legend.

At late times, the progenitor candidate for AT 2016jbu is still present. In 2019, over two years since the epoch of maximum light, a source is found at approximately the same *F814W* magnitude as was seen in 2006. It is unlikely that this source is a compact cluster, as the pre-explosion photometric variability can only be explained if a single star is contributing most of the flux. Moreover, we compared the 2006 *F814W* and 2019 *F814W* images and find that the position of the source is consistent to within 17 mas between the two epochs. This implies that the same source is likely dominating the emission at both epochs, and if there is an underlying cluster it must be much fainter than the progenitor source.

2.2 Physical properties of the progenitor

In order to determine the luminosity and effective temperature of the progenitor of AT 2016jbu, we consider the WFC3 photometry taken in early 2016. As a first step, we normalize out the variability seen over this period so that we can build an SED from photometry

Downloaded from https://academic.oup.com/mnras/article/513/4/5666/6581584 by University of Arizona user on 02 September 2022

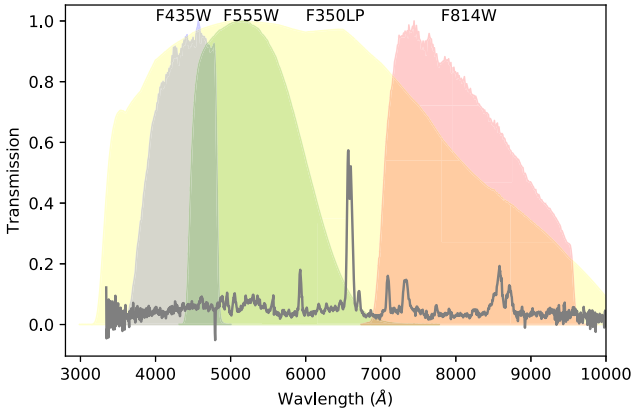

Figure 3. *HST* filters used for the pre-explosion light curve, compared with the +271 d spectrum. Only *F350LP* covers the strong Hα emission seen at this epoch.

taken in different filters at different epochs. To do this, we fit a linear function to the colour curves of our *HST* observations. We disregard the first epoch for the *F350LP*−*F160W* colour (which is significantly redder than the other epochs); this measurement is unreliable, as the progenitor was affected by bad pixels in two of the three individual exposures. We then use the fitted functions to interpolate or extrapolate the magnitude of AT 2016jbu in *F555W*, *F814W*, or *F160W* as necessary. Finally, we shift the SEDs up or down in magnitude so that they all have the same *F814W* magnitude as the 2006 value. The resulting normalized progenitor SEDs can be seen in Fig. 4.

In order to determine a progenitor temperature from the observed SED, we compare the progenitor SED with MARCS stellar atmosphere models (Gustafsson et al. 2008). We used the PYSYNPHOT package to perform synthetic photometry on the surface fluxes of the models and hence calculate their magnitude in each of the *F555W*, *F814W*, and *F160W* filters. We shifted each model so that it matches the 2006 MW extinction-corrected *F814W* absolute magnitude of the progenitor. In the lower panel of Fig. 4 we compare the progenitor SED with the spherically symmetric MARCS models for 15-$M_\odot$ red supergiants (RSGs: $\log(g) = 0$) at solar metallicity. While we can see that the models provide reasonable agreement, it is clear that the warmest model (at 4500 K) is still too red to match the *F555*−*F814W* colour of the progenitor, implying that the progenitor is hotter than this. Conversely, the 4000-K model provides a good match to the *F814W*−*F160W* colours of the progenitor. As the 15-$M_\odot$ supergiant models cover a relatively small temperature range, we also explored the 5-$M_\odot$ spherically symmetric MARCS models at $\log(g) = 1.0$, which span a broader range (upper panel in Fig. 4). We find that a 5000-K model can reproduce the optical colours of the progenitor, while the NIR is better matched with a cooler 4000-K model.

While AT 2016jbu does not appear to suffer from high levels of circumstellar extinction around maximum light, we cannot exclude the possibility that the progenitor colours are caused by close-in CSM dust that was subsequently destroyed. To explore this possibility, we used the DUSTY (Ivezic & Elitzur 1997) code to calculate observed SEDs for a grid of progenitor models allowing for different levels of CSM dust. DUSTY solves for radiation transport within a dusty medium.

Since a dust-enshrouded progenitor could be hotter than the range of temperatures covered by the MARCS model grid, we used the

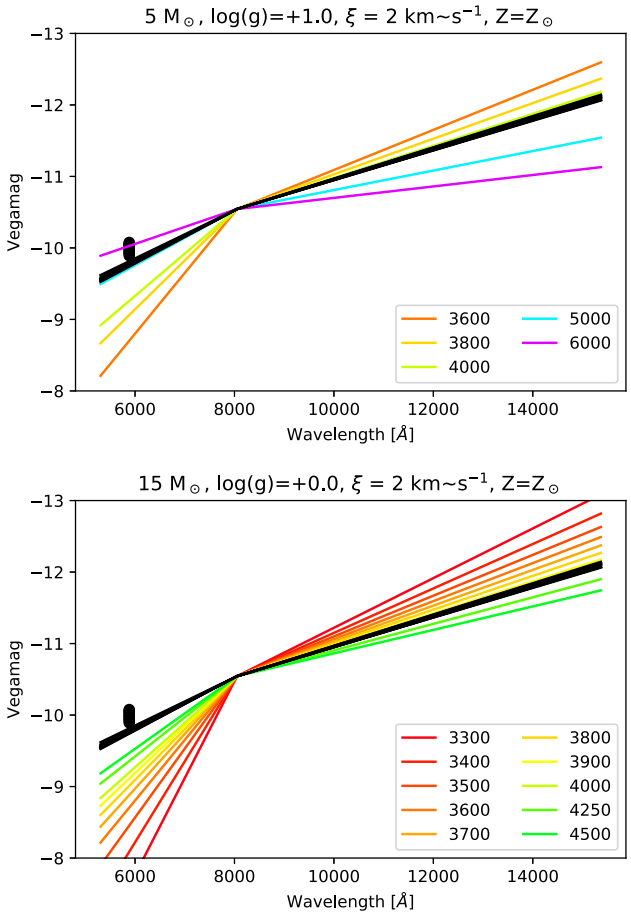

Figure 4. *HST* SEDs for AT 2016jbu based on the early 2016 WFC3 imaging are shown in black. All SEDs have been shifted so that their *F814W* magnitudes match, as discussed in the text. The *F350LP* filter magnitudes have not been included in the SED as they are strongly affected by Hα emission. We also plot a number of SEDs derived from MARCS models. In the lower panel we show the 15-$M_\odot$ MARCS models appropriate to cool red supergiants. As this model grid does not extend above 4500 K, we also plot a set of 5-$M_\odot$ models with slightly higher $\log(g)$ in the upper panel. All models have been shifted so that they match the *F814W* filter magnitude of the progenitor, and we can see that, while the cooler models can match the NIR part of the SED, hotter temperatures are required to match the optical.

PHOENIX models[4] (Husser et al. 2013) as our input spectra. The PHOENIX models cover the temperature range from 6000–12 000 K in 200-K increments, and have $\log(g)$ between 1 and 2 dex. MARCS models covering a temperature range from 2600–7000 K in 100-K increments and with $\log(g)$ between 1 and 2 dex were also tested as input to DUSTY. These models were then processed by DUSTY, assuming spherically symmetric dust comprised of 50 per cent silicates and 50 per cent amorphous carbon. The dust density followed a r^{-2} distribution, with a radial extent varying between 1.5 and 20 times the inner radius of the dust shell. The dust mass is parameterized in terms of the optical depth in the V band, τ_V, which varies between 0 and 5. We expect the dust temperature to be relatively hot (Foley et al. 2011; Smith et al. 2013). We vary the dust temperature at the inner dust boundary between 1250 and 2250 K. For each temperature and dust combination, we calculated synthetic $F555W - F814W$ and

[4] http://phoenix.astro.physik.uni-goettingen.de

Downloaded from https://academic.oup.com/mnras/article/513/4/5666/6581584 by University of Arizona user on 02 September 2022

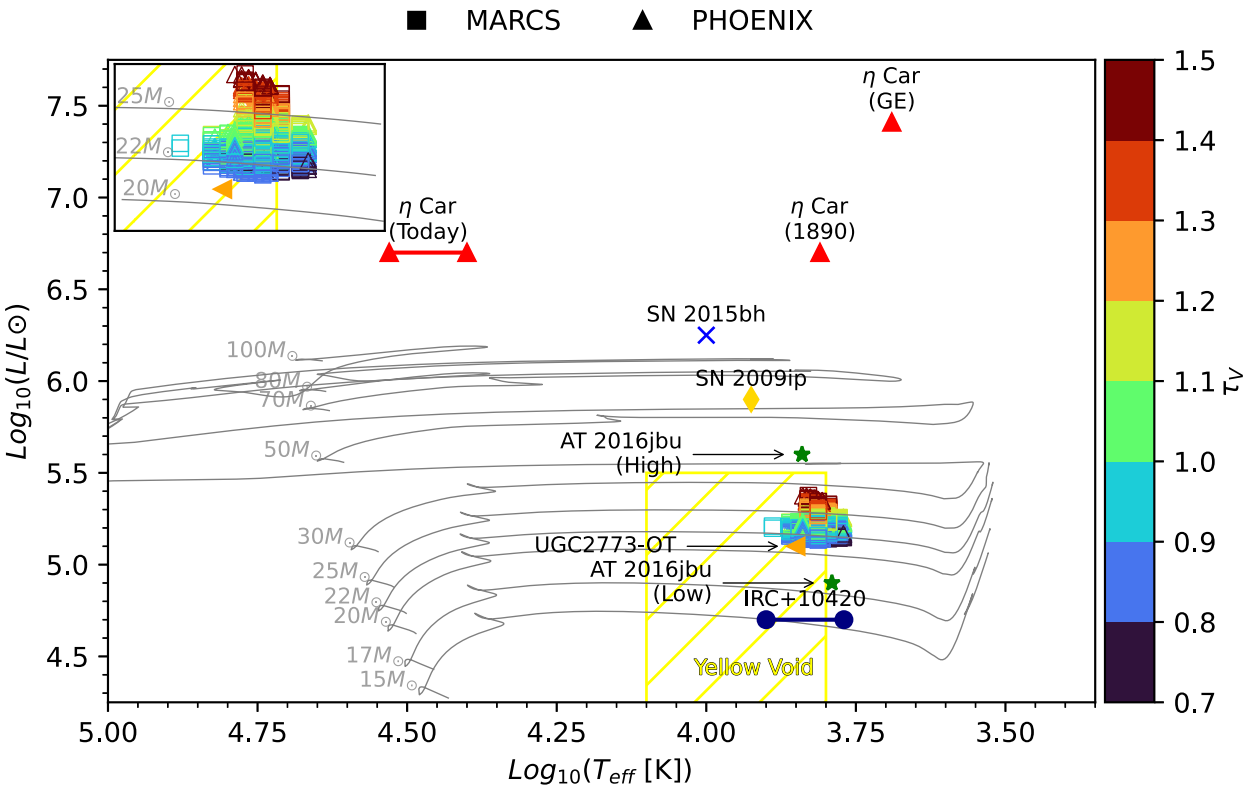

Figure 5. Hertzsprung–Russell (HR) diagram showing single-star evolutionary tracks from BPASS (Eldridge et al. 2017; Stanway & Eldridge 2018). We include SN 2009ip at $\log(L/L_{\odot}) = 5.9$ and $\log(T_{\rm eff}) = 3.92$ (Smith et al. 2010; Foley et al. 2011), as well as SN 2015bh (Boian & Groh 2018), IRC + 10420 (Klochkova et al. 2016), and UGC 2773−OT (Smith et al. 2015). η Car is plotted (red triangles) at several phases given in parentheses (Prieto et al. 2014). We include the progenitor estimates for AT 2016jbu from K18, in both the 'low' and 'high' states, as green stars. We highlight the Yellow Void between 7000 and 10 000 K (de Jager 1998) and include the output of our DUSTY modelling for AT 2016jbu using *PHOENIX* models (multi-coloured triangles) and *MARCS* models (multi-coloured squares). The colour of each point corresponds to its optical depth (τ_v), which is provided on the colour bar on the right. We include an inset of the region around the progenitor in the top left of the plot.

$F814W - F160W$ colours and compared these with the foreground extinction-corrected colours of the AT 2016jbu progenitor. In Fig. 5 we plot all models that have colours within 0.1 mag of the progenitor.

We find that we are able to match the progenitor colours with models with temperatures of between $10^{3.7}$ and $10^{3.9}$ K, for a circumstellar dust shell with optical depth τ_V between 0.7 and 1.5 and dust temperature between 1500 and 2000 K, in agreement with what was seen in the environment of SN 2009ip (Smith et al. 2013), as well as the SN imposter UGC 2773−OT (Foley et al. 2011). Additionally, we find little influence of the radial extent of the dust on matching models.

We calculated a luminosity for each of these models by integrating over its spectrum, and find that the progenitor had a luminosity $\log(L)$ between 5.1 and 5.3 dex (depending on temperature and extinction). Comparing this with the Binary Population and Spectral Synthesis (BPASS) single-star evolutionary tracks at solar metallicity in Fig. 5, we find that these correspond to approximately the luminosity of a 22–25 $M_{\odot}$ star as it crosses the HR diagram to become a RSG. We plot the DUSTY models that match our progenitor measurements in Fig. 5.

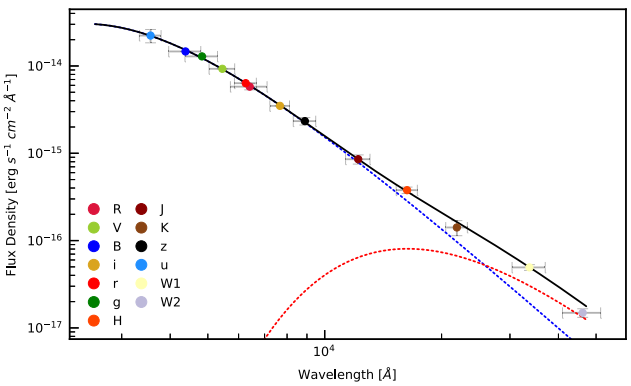

Figure 6. SED fit of AT 2016jbu at −11 days before *Event B* maximum. Extinction-corrected photometry is grouped into 1-day bins and weight-averaged. Flux errors are given as standard deviation of bins. Horizontal error bars represent the approximate filter band-pass. The hot blackbody is given in blue, the cooler blackbody in red, and the black line is a compound model. We note a similarity with the SED for SN 2009ip presented in Margutti et al. (2014).

3 EVIDENCE FOR DUST

We present a SED model fitted to our −11 day dataset in Fig. 6. We fit at this phase as it has the broadest wavelength coverage without the need for interpolation. We fit two blackbody models to the photometric points: one representing a hot photosphere and the second fitted to the IR excess seen in *H*, *K*, *W*1, and *W*2. A single blackbody does not fit observations seen at −11 d before maximum. Allowing for a second cooler blackbody at a larger radius gives a model that fits the data well. This additional blackbody is

Downloaded from https://academic.oup.com/mnras/article/513/4/5666/6581584 by University of Arizona user on 02 September 2022

consistent with warm dusty material at a distance of 170 au and a temperature of $T_{\rm BB}$ ∼1700 K. This material provides an additional luminosity of 2.7×10^7 L$_\odot$. The hot blackbody has a radius of 36 au, a temperature of $T_{\rm BB} \sim 12\,000$ K, and an integrated luminosity of 1.3×10^8 L$_\odot$, and represents $R_{\rm BB}$ at this time. We find a dust mass of $M_{\rm dust} \approx 2.27 \times 10^{-6}$ M$_\odot$ (using equation 1 from Foley et al. 2011). In comparison, Smith, Mauerhan & Prieto (2014) find a lower dust mass of (3–6) $\times 10^{-7}$ M$_\odot$ for SN 2009ip. Additionally, we note a similarity to the SED for SN 2009ip presented in Margutti et al. (2014). The IR excess may be caused by thermal radiation of pre-existing dust in the CSM reheated by an eruption at the beginning of *Event B*, i.e. an IR echo. We can compute the radius within which any dust will be evaporated/vaporized at the phase of our SED fitting. The radius of this dust-free cavity is given by

$$R_{\rm c} = \sqrt{\frac{L_{\rm SN}}{16\pi\sigma T_{\rm evap}^4 \langle Q \rangle}}, \quad (1)$$

where $R_{\rm c}$ is the cavity radius, $L_{\rm SN}$ is the luminosity of the transient, taken to be 1.3×10^8 L$_\odot$, σ is the Stefan–Boltzmann constant and $\langle Q \rangle$ is the averaged value of the dust emissivity. Assuming radiation is absorbed with efficiency ∼unity by the dust, we find a cavity radius of ∼ 245 au for graphite grains ($T_{\rm evap} = 1900$ K) and ∼ 400 au for silicate grains ($T_{\rm evap} = 1500$ K). Both values are significantly larger than that from our warm blackbody radius (∼ 170 au). A dust destruction radius larger than the blackbody radius of our putative warm dust component appears at first glance to be inconsistent. To ameliorate this, we suggest that the dust may not be homogeneously distributed and could be in either optical clumps or an aspherical region that provides some shielding from evaporation. Over time, we expect that the dust will be further heated and destroyed during the rise to *Event B* maximum. We find that, by maximum brightness, this additional blackbody component is no longer needed, suggesting that the dust causing this NIR excess has been destroyed. As discussed in Paper I, as well as K18, there are *Spitzer* + IRAC observations of the progenitor site of AT 2016jbu, which show tentative detections in 2003 and 2018. Using 2003 *Spitzer*/IRAC and 2016 *HST*/F160W observations, K18 find fits consistent with a compact dusty CSM component with mass $M_{\rm dust} \approx 7.7 \times 10^{-7}$ M$_\odot$ at 72 au. This may represent a dusty shell that is later seen as our 170-au warm blackbody. However, due to the timeframe between Spitzer/*HST* observations, there are large uncertainties in dust parameters from K18. Fitting *Spitzer* data only gives a slightly higher $M_{\rm dust}$ value of $\sim 10^{-6}$ M$_\odot$ at 120 au. Due to the erratic variability seen in AT 2016jbu, it is uncertain as to whether these dust shells are the same, as AT 2016jbu may have a stratified CSM environment resulting from successive outbursts. Although there is strong evidence for pre-existing dust, we do not see any signature for newly formed dust in the environment around AT 2016jbu (Meikle et al. 2007; Smith, Foley & Filippenko 2008; Smith 2011). We see no NIR excess in late-time *J* and *K* bands in late-time photometry, nor an IR excess evident in spectra. Furthermore, there is no blueshift in the core emission component in Hα (Paper I), which is another indicator of newly formed dust.

4 THE ENVIRONMENT OF AT 2016JBU

Along with direct detections of progenitors, analysis of the resolved stellar population in the vicinity of a SN has also been used to infer the progenitor age and hence initial mass (Gogarten et al. 2009; Maund 2017; Williams et al. 2018). An advantage to this technique is that it will not be affected by any peculiar evolutionary history or variability of the progenitor that may cause it to appear less or more massive than it truly is. On the other hand, using the environment around a SN is an indirect proxy for the progenitor age, and is predicated on the assumption that the local stellar population is coeval. This method is also complicated by possible contamination from other stellar populations from multiple star formation episodes.

4.1 *Hubble Space Telescope* imaging of the environment

In order to study the population in the vicinity of AT 2016jbu, we require sources to be matched between different filter images. While this is straightforward for bright sources such as the progenitor of AT 2016jbu, it is more challenging for fainter or blended sources, especially when images have different pixel scales or orientations. We hence re-ran the photometry on a subset of the *HST* images (*F435W*, *F658N*, and *F814W* from 2006 October 20; *F350LP* and *F555W* from 2016 January 31), using a single drizzled ACS *F814W* image as the reference image for all filters.

We chose a projected radius of 150 pc (1.48 arcsec) around AT 2016jbu as a compromise between identifying sufficient stars to be able to constrain the population age and ensuring we are still sampling a local population that is plausibly coeval with the progenitor. We also create a less restrictive catalogue of sources within a projected distance of 300 pc from AT 2016jbu, as well as a more limited catalogue of sources within 50 pc. After applying cuts to select only sources with a point-source PSF, DOLPHOT detects 84 sources at signal-to-noise ratio (S/N) >3 within 150 pc of AT 2016jbu and 255 sources within 300 pc.

In Fig. 7 we compare our 50-, 150-, and 300-pc populations with a set of the PAdova and TRieste Stellar Evolution Code (PARSEC) isochrones[5] (Marigo et al. 2017; Bressan et al. 2012) in three different filter/colour combinations. We use the most recent version of the PARSEC models (version 1.2S: Chen et al. 2015) and, for the purposes of the comparison, we have applied our foreground reddening and distance modulus to the PARSEC models.

The progenitor of AT 2016jbu clearly stands out from the local population, in terms of both its bright apparent magnitude and its unusual colours. The colour of AT 2016jbu should not be compared with these isochrones; not only will the *F350LP* filter be strongly affected by Hα emission but, as the various filter combinations plotted do not come from contemporaneous data, the variability seen in the progenitor will affect the apparent colour significantly.

Turning to the 150-pc population, it is clear that no source is found to be brighter than the 10-Myr isochrone, constraining the population to be older than this. We find a similar result looking at the wider environment within 300 pc of AT 2016jbu, as well as the closer-in population within 50 pc.

Using the AGEWIZARD and BPASS models (Eldridge et al. 2017; Stevance, Eldridge & Stanway 2020a; Stevance et al. 2020b), we obtain a probability distribution for the age of the resolved stellar population within 150 pc around AT 2016jbu (see Fig. 8). The 90 per cent confidence interval is found to be 15–200 Myr. Additionally, we can ascertain that the neighbouring population of AT 2016jbu is older than 10 Myr (5 Myr) with over 95 (99.8) per cent confidence.

Therefore, there is no evidence for a very young environment, which would be expected for an 80- (or even 150-) M$_\odot$ progenitor, as proposed for SN 2009ip and η Car (Smith et al. 2010; Foley et al. 2011).

[5] http://stev.oapd.inaf.it/cgi-bin/cmd

Downloaded from https://academic.oup.com/mnras/article/513/4/5666/6581584 by University of Arizona user on 02 September 2022

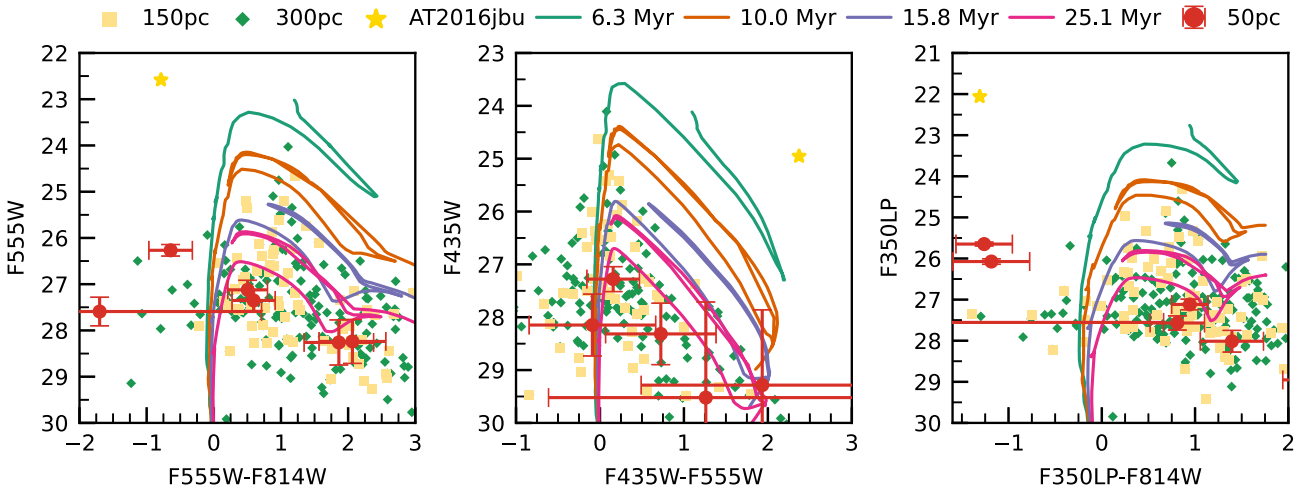

Figure 7. Colour–magnitude diagram (CMD) of the stellar population around the site of AT 2016jbu. We show three different colour combinations, each with PARSEC isochrones with population ages (solid coloured lines) given in the upper legend. Yellow squares are point sources within 150 pc and green diamonds are sources within 300 pc, while sources within 50 pc of the progenitor are plotted in red with error bars. The progenitor of AT 2016jbu from the early 2016 *HST* observations is given as a gold star in each panel.

4.2 *MUSE*-ing on the local environment

We further investigate the nature of AT 2016jbu by looking at its local environment in Integral Field Unit (IFU) data. AT 2016jbu was observed on 2017 December 2 (+303 d) using the VLT equipped with the MUSE instrument in Wide Field Mode. The date cube was obtained as part of a survey of SN late-time spectra in conjunction with the AMUSING survey of SN environments (Galbany et al. 2016; Kuncarayakti et al. 2020). We downloaded the pre-calibrated data cubes from the ESO archive and present our data analysis for the environment around AT 2016jbu in Fig. 9.

We fit for spectral features at each spaxel using a Gaussian emission profile with a linear pseudo-continuum over a small wavelength range. For measuring the ratio of Hα and Hβ for the extinction map, we constrain the ratio of the two emission lines such that Hα/H$\beta \leq 2.85$ (Case B recombination). To exclude the effects of AT 2016jbu on the analysis, we exclude any pixel within 3 arcsec of AT 2016jbu. We do not account for any stellar absorption effects and, as such, values here are lower limits. For completeness, we include the extracted spectrum of AT 2016jbu in Fig. 10.

We show the extinction map across the field of view (FOV) using the method in Domínguez et al. (2013), measured using the Balmer decrement. A proxy for the star formation rate (SFR) is measured using $L_{\mathrm{H}\alpha}$ (Kennicutt 1998). $L_{\mathrm{H}\alpha}$ was corrected for extinction using the Balmer decrement (Vale Asari et al. 2020). We also plot a metallicity map using the metallicity indicators given by Dopita et al. (2016).

Fig. 9 does not include the core of the host galaxy, nor the southern arm. AT 2016jbu is located north of the southern distorted spiral arm of NGC 2442 and is still clearly present in NGC 2442 almost a year after maximum, as seen in the white-light image constructed from the datacube. The FOV (1×1 arcmin^2) does, however, include the location of SN 1999ga (Pastorello et al. 2009), as well as a luminous region in the centre frame. This '*Super-Bubble*' has been noted by previous authors (Pancoast et al. 2010) and is seen in the irregular kinematic pattern seen in the centre of the FOV. Placing an age on this region is difficult, but it is likely to have formed within the last 150–250 Myr (Mihos & Bothun 1997). This is a spherical-looking area within the diffuse region to the south-west of the nuclear region, with a diameter of ~ 1.7 kpc.

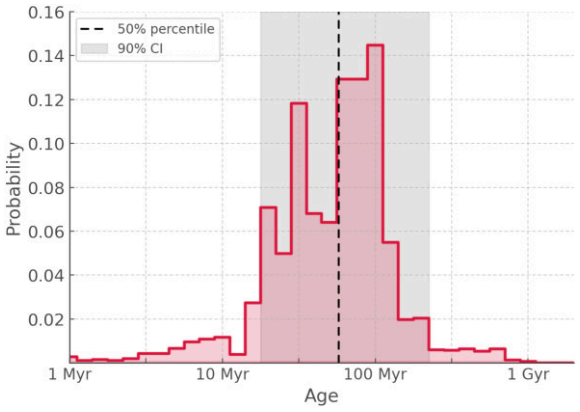

Figure 8. Probability distribution of the age of the 150-pc stellar neighbourhood of AT 2016jbu found using AgeWizard. The 90 per cent confidence interval is highlighted in grey.

This Super-Bubble region is in the vicinity of both AT 2016jbu and SN 1999ga (Ryder et al. 2001; Pastorello et al. 2008; Pancoast et al. 2010). This region shows a high SFR and is bright in the *B* band, both signs of massive star formation. High SFR is linked with a high SN rate (Botticella et al. 2012) and it is a fair assumption that the general location of this Super-Bubble is likely to host CCSNe, as is obvious from SN 1999ga.

The top middle panel in Fig. 9 maps the extinction across the FOV using the Balmer decrement (Domínguez et al. 2013). We find a value for the local extinction ($E_{B-V} < 0.45$) within 500 pc of AT 2016jbu, with a similar value seen across the FOV. The top right panel in Fig. 9 gives the velocity dispersion across the FOV. The location of AT 2016jbu lies in an area moving at ~ -100 km s^{-1} (image corrected for redshift: $z = 0.00489$). The bottom left panel shows a pseudo-SFR based on the extinction-corrected Hα emission (Kennicutt 1998). The figure shows two bright regions of star formation, which is clear from the white-light image. AT 2016jbu is situated on the outskirts of a moderate star-forming region, $\sim 10^{-6}$ M$_\odot$ yr^{-1}. SN 1999ga lies on the edge of the brighter star-forming region. We include a metallicity map (bottom right panel) following the metallicity indicators from

Downloaded from https://academic.oup.com/mnras/article/513/4/5666/6581584 by University of Arizona user on 02 September 2022

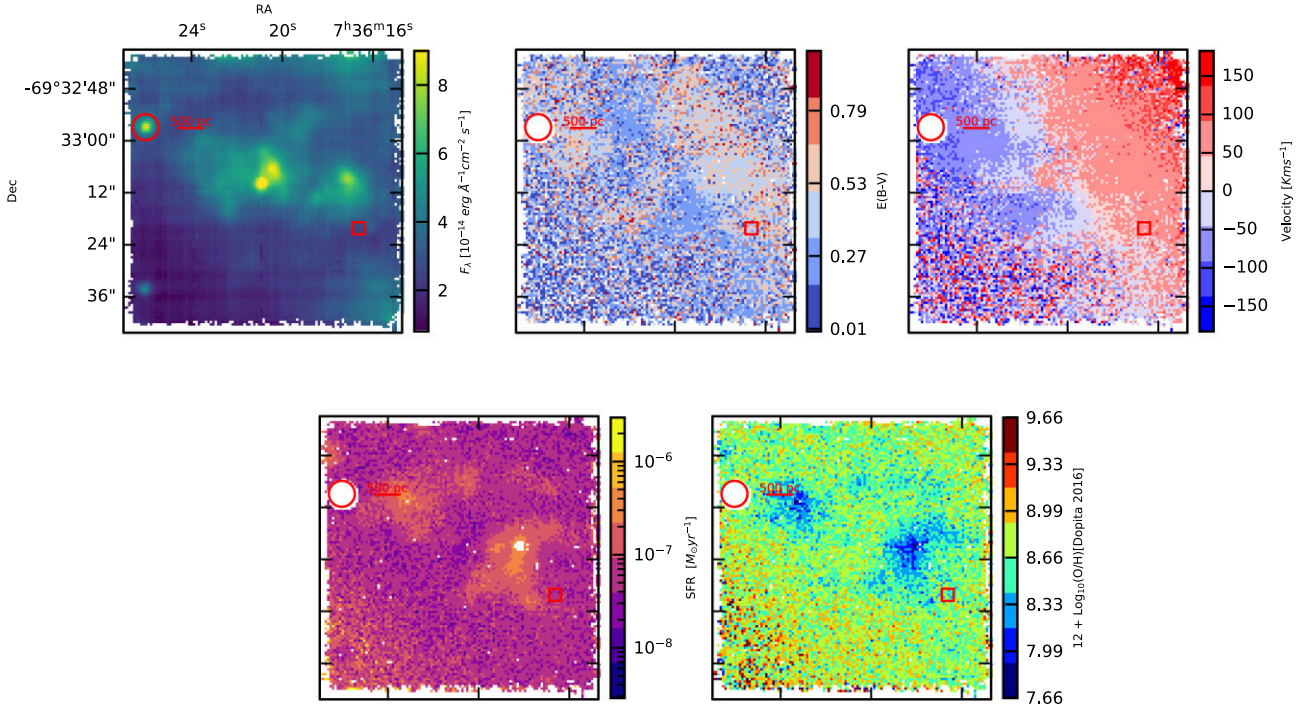

Figure 9. IFU analysis of the environment of AT 2016jbu. The spectral cube was corrected for Milky Way extinction and redshift. Observations were taken on 2017 December 2 (+303 d). Data are orientated such that north is up and east is to the left. Included in each panel is a horizontal scale bar showing 500 pc. We include a white-light image (5000–7000Å; top left), an extinction map (top middle) based on Domínguez et al. (2013), a velocity field plot from Hα corrected for recessional velocity (top right), the star formation rate based on Kennicutt (1998; bottom left) and a metallicity map (bottom right) based on Dopita et al. (2016). The location of AT 2016jbu is marked with a red circle of radius 3 arcsec. We also include the location of SN 1999ga as a square to the south-west of AT 2016jbu. Data are not shown where EW < 1 Å or within 3 arcsec of AT 2016jbu.

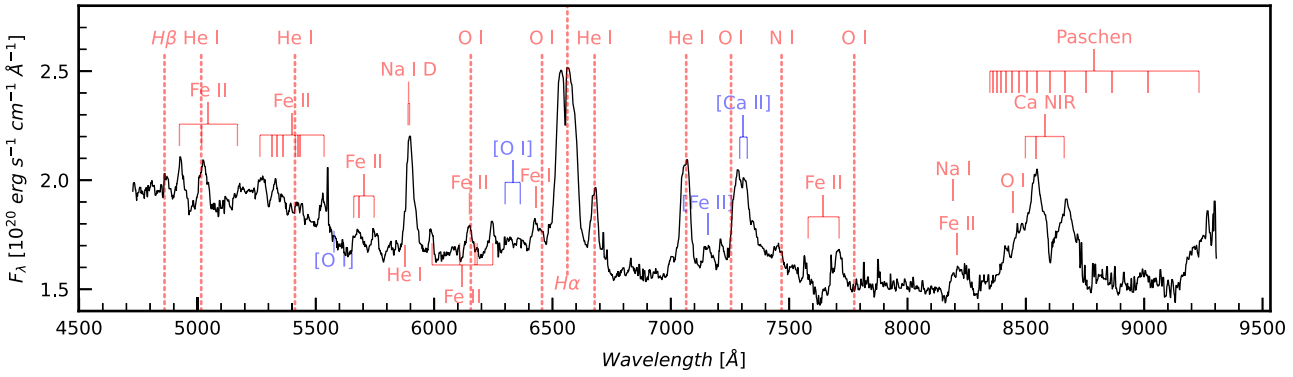

Figure 10. Extracted spectrum of AT 2016jbu from VLT + MUSE. The spectrum was extracted using a 1-arcsec aperture at the transient position and corrected for redshift and Galactic extinction. We mark strong emission features in red and several forbidden transition lines are marked in blue. The transient appears relatively blue even at ∼ +10 months, a possible sign of ongoing interaction.

Dopita et al. (2016). The full FOV yields an approximately solar environment, with median metallicity across the field of 8.66 dex ($Z \approx 0.015$).

5 BOLOMETRIC EVOLUTION OF AT 2016JBU

The bolometric light curve for AT 2016jbu is computed using *ugiz*, *UBVR*, *JHK*, *Gaia G*, *W*1, and *W*2 from *WISE*, as well as *Swift* + UVOT *UVW2*, *UVM2*, *UVW1*, *U*, *B*, and *V*. All calculations were carried out using SUPERBOL[6] (Version 1.7; Nicholl 2018). Effective wavelengths were taken from Fukugita et al. (1996) and zero-point flux energies were taken from Tonry et al. (2018), while SUPERBOL was modified to also handle our *WISE* data. Extinction values in each filter were computed using the York Extinction Solver (McCall 2004). All magnitudes were converted to F_λ and interpolated where necessary to account for epochs without specific filter coverage, taking the *r* band as the reference filter. Blackbody fitting is performed for photometric bands that are centred on $\lambda > 3000$ Å to avoid the effects of strong line-blanketing. We also obtain a pseudo-bolometric light curve by integrating F_λ directly using the trapezoidal rule between 0.2 and 4.5 μm (*UVW2* to *W2*). We present the results of our blackbody fitting in Fig. 11.

[6]https://github.com/mnicholl/superbol

Downloaded from https://academic.oup.com/mnras/article/513/4/5666/6581584 by University of Arizona user on 02 September 2022

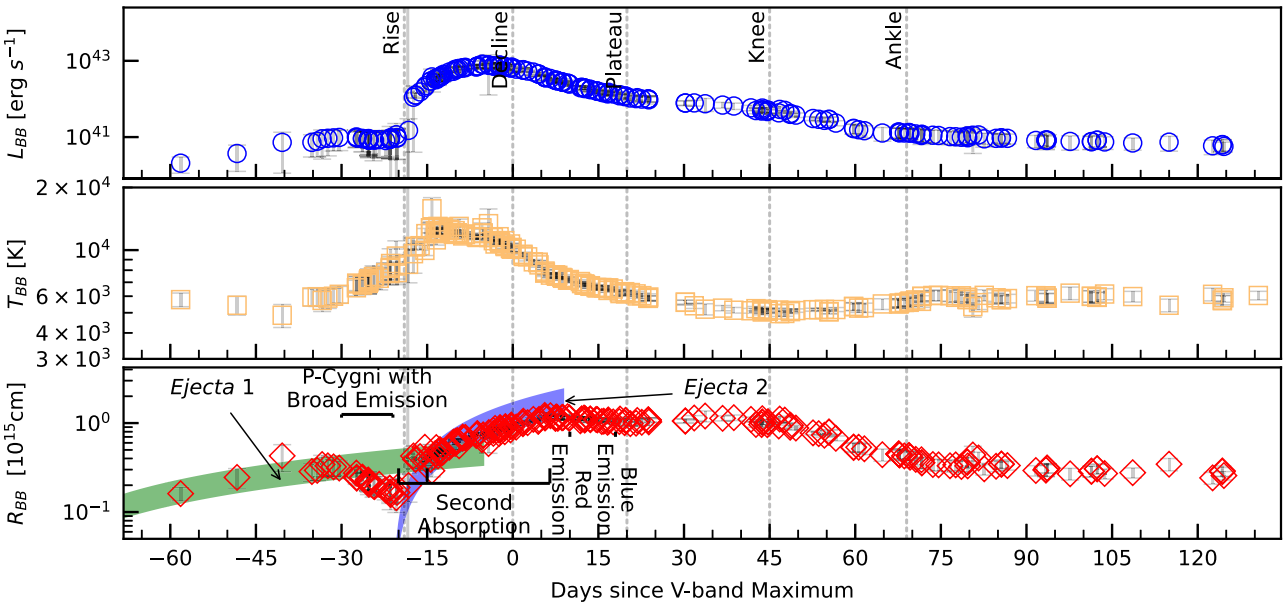

Figure 11. Blackbody luminosity (top panel), temperature (middle panel), and radius (lower panel) of AT 2016jbu calculated using SUPERBOL (Nicholl 2018). In the second and third panel, we include T_{BB} and R_{BB} fits to our optical spectra (Paper I). We include approximate epochs where specific Hα features emerge in the R_{BB} panel, as discussed in the text. The green shaded region shows the linear distance travelled by the slower moving material, *Ejecta 1*, causing the P Cygni absorption. The blue shaded region is the same for the faster moving material, *Ejecta 2*. The lower and upper bounds for each band are bulk and max velocities, respectively.

AT 2016jbu is an interacting transient showing strong emission lines. Interpreting the blackbody evolution of photometry alone may be misleading, due to the uncertainty as to whether the photometry is continuum-dominated or line-dominated. For completeness, we investigate blackbody fits from our optical spectra. A blackbody function was fitted to the optical spectra presented in Paper I while excluding strong emission features and only fitting for $\lambda > 3000$ Å. We find excellent agreement with the blackbody evolution from photometric and spectroscopic data until $\sim +125$ d. After this time, our observations become strongly line-dominated and blackbody fitting becomes unreliable.

5.1 Radius and kinematics

We show the blackbody luminosity (L_{BB}), radius (R_{BB}), and temperature (T_{BB}) fits from SUPERBOL in Fig. 11. The H emission for AT 2016jbu shows two distinct absorption components (see Paper I). The first component is seen in a P Cygni profile that is present up until $\sim$0.5 years after the *Event B* maximum. The second component is present for $\sim$1 month with respect to its first emergence, and suggests some absorbing, high-velocity (HV) material. A similar feature has been seen in other SN impostors (e.g. Tartaglia et al. 2016b) and is common in SN 2009ip-like transients. The presence of two regions of material with different velocities lends credence to the idea that interaction with some material during, or prior to, *Event A* is the main source of energy input for *Event B* (Fraser et al. 2013a; Benetti et al. 2016; Elias-Rosa et al. 2016; Thöne et al. 2017).

To explore this scenario further, we assume some optically thick material causing the P Cygni absorption was ejected at ~ -90 d (first detection of *Event A*, see Paper I), although this ejection may have occurred earlier.

Fitting a P Cygni absorption profile gives a maximum velocity of ~ -850 km s^{-1}, with a bulk velocity of ~ -600 km s^{-1} for the slower absorption feature seen in the Balmer lines. We refer to this material as *Ejecta 1*. The higher velocity absorption (which we refer to as *Ejecta 2*) has a maximum velocity from the blue edge of the line of $\sim -10\,000$ km s^{-1}, with the bulk of the material at ~ -4500 km s^{-1}. Using these velocities, we attempt to constrain ejection/collision times.

The ejection epoch for the material causing the second high-velocity absorption component is open to debate. There is no evidence for this additional absorption in optical spectra at -24 d and it is only seen at -15 d. Under the presumption that we do not see this shell of material (i.e *Ejecta 2*) until it interacts with the pre-existing material or until it is no longer occulted by an existing photosphere, we find that a shell moving at $\sim$4500 km s^{-1} for $\sim$3 days can reach a distance of $R_{BB} \sim 0.1 \times 10^{15}$ cm. We include the distance travelled by *Ejecta 2* in Fig. 11 as a blue band. We can constrain the ejection date of this HV material to $\sim$21 days before maximum light, with the collision date (when *Ejecta 2* catches up to *Ejecta 1*) at $\sim$19 days before maximum light.

We draw attention to the blackbody evolution over the period -19 d to -13 d. During this timeframe, we see an inflection between the decline of *Event A* and the rise of *Event B*. Although we have low-cadence coverage during *Event A*, the distance travelled by *Ejecta 1* follows R_{BB} quite well during *Event A*. R_{BB} then contracts slightly, beginning around -30 d, to a minimum at -19 d. At ~ -19 d, R_{BB} increases at a velocity similar to the velocity profile of *Ejecta 2*. This implies that the blackbody radius now follows this material, which is likely *Ejecta 2* with additional material swept up from *Ejecta 1* and some CSM material. While this is undoubtedly a simplified picture, it appear that AT 2016jbu is potentially consistent with two successive eruptions (either non-terminal or a CCSN) where the collision of ejecta powers the luminosity of *Event B*.

We initially find T_{BB} at $\sim$5700 K, which is roughly constant up until ~ -30 d. T_{BB} evolves exponentially from 6000 K at -30 d to 12 000 K at -12 d. After the *Event B* maximum (marked as *Decline*

Downloaded from https://academic.oup.com/mnras/article/513/4/5666/6581584 by University of Arizona user on 02 September 2022

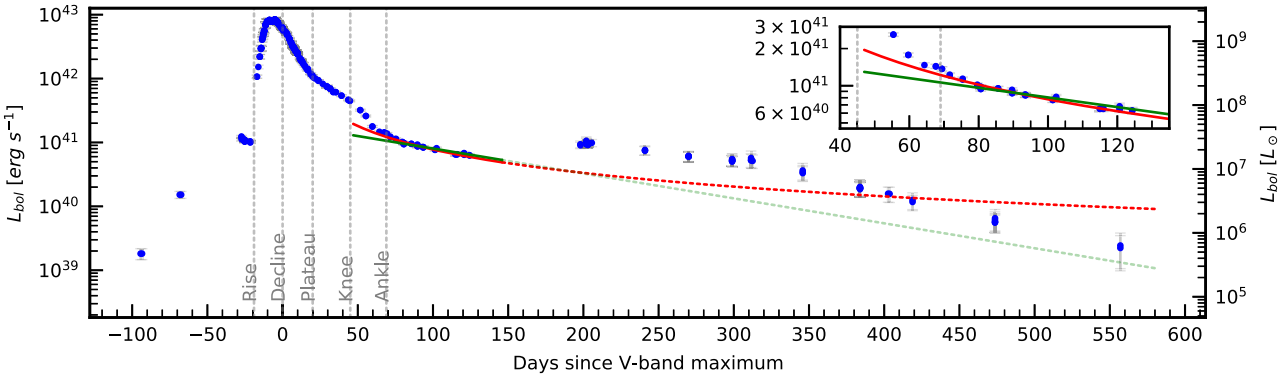

Figure 12. Pseudo-bolometric luminosity of AT 2016jbu using SUPERBOL (Nicholl 2018). We include the luminosity shock function (equation 4; solid red line) and a radioactive decay tail fit (green solid line). Both functions are extrapolated until the end of observations (dashed lines). Both functions are fitted to the post-ankle stage and we include a zoom-in of this area in the top right. We find a ^{56}Ni mass of 0.016 M$_\odot$ (assuming the SN explosion date as −21 d) and $\dot{M}$ is 0.05 M$_\odot$ yr^{-1} for equation (4).

in Fig. 11), T_{BB} cools to ∼5100 K at the *Knee* epoch and increases slightly to ∼6000 K at the beginning of the *Ankle* epoch.

It is important to note that we see both components in spectra during the first month of *Event B*. Additionally, the full-width at half-maximum (FWHM) and velocity offset do not evolve significantly during the first few months (see Paper I).

This is likely due to *Ejecta 1* or the CSM or both being highly asymmetric. We are motivated by the spectral evolution of the Hα profile, the evolution of R_{BB}, and the degenerate appearance of the Hα emission lines in SN 2009ip-like objects; see Paper I for further discussion. If *Ejecta 2* is spherically symmetric (e.g. possibly a CCSNe), some material of *Ejecta 2* would not interact with *Ejecta 1* and expand freely along the lower density regions.

We include labels indicating when certain spectral components appear in Hα in Fig. 11, bottom panel. We see that the HV blue absorption feature coincides with the evolution of *Ejecta 2*; this absorption is clearly seen at −18 d and is detected until +5 d with fitting-model-dependent tentative detections up to +10 d. This second absorption component appears during the rise in R_{BB} during *Event B* and vanishes when R_{BB} reaches its maximum at ∼+7 d. At ∼ + 9 d, R_{BB} remains at a constant value and we see the emergence of broad, red shoulder emission in Hα at ∼ 1400 km s^{-1}, FWHM ∼ 4000 km s^{-1}. This may follow material expanding at ∼1400 km s^{-1}, a receding photosphere, or both. Several days later, the blue emission feature appears in Hα and remains until late times. At +18d this blue emission is centred at ∼ −2400 km s^{-1} with FWHM ∼3800 km s^{-1}.

Photons from the interaction site between *Ejecta 2* and *Ejecta 1*/CSM may be diffusing outwards at this epoch. We see that the red shoulder emission only appears after R_{BB} reaches its maximum values, shortly followed by the blue shoulder emission a week later. This leads to our conclusion that *Ejecta 1* is partially asymmetric and, when *Ejecta 2* collides with it, *Ejecta 1* is partially engulfed. The interaction between these two shells then becomes apparent at ∼ + 7 d, when asymmetric emission features are clearly seen in Hα.

R_{BB} peaks at 1.2 × 10^{15} cm, at ∼1 week after *Event B* maximum, and remains roughly constant until the *Knee* phase. Thereafter, there is a drop of ∼−5 × 10^{13} cm per day until the beginning of the *Ankle* phase. R_{BB} remains roughly constant at ∼0.3 × 10^{15} cm up until the seasonal gap begins at +140 d. This epoch coincides with a narrowing of both red and blue emission features and an increase in equivalent width (EW) of both components. This may represent a time when opacities drop significantly and there is less photon scattering. Using this collision scenario as the dominant energy input for this transient, we will explore the necessary energy budget in Section 6. Using the evolution of R_{BB}, we can understand the nature of the explosion of AT 2016jbu better, and we will discuss this further in Section 7.2.

6 POWERING AT 2016JBU

The nature of the energy input of AT 2016jbu and SN 2009ip-like transients is debated. If AT 2016jbu is indeed a CCSN, then this energy comes from an imploding iron core and the early light curve is powered by the fast-moving SN ejecta material. Ejecta interacting with a dense CSM can power the light curve for many years (see Fraser 2020, and references therein). If the transient is a CCSN, after the ejecta expands and cools, the late-time light curve is powered by the radioactive decay of ^{56}Ni. We discuss the possible presence of ^{56}Ni in Section 6.1.

If AT 2016jbu is a CCSN, then it is spectroscopically classed as Type IIn, meaning we see strong signs of interaction with a dense, slow-moving CSM. We discuss the energy input from ejecta/CSM interaction in Section 6.2.

6.1 ^{56} Ni mass

A product of CCSNe is explosively synthesized radioactive ^{56}Ni, the decay of which can power the late-time light curve of H-rich supernovae, after the hydrogen ejecta have recombined fully and any additional interaction has stopped. Anderson (2019) find that, for H-rich, Type II SNe, the median value for the amount of ^{56}Ni synthesized is 0.032 M$_\odot$. We show our attempt to fit for a nickel decay tail in Fig. 12 (green dashed line). We find that the pseudo-bolometric light curve shows a decay that is consistent with that of radioactive nickel during the *Ankle* stage.

Determining an explosion epoch for AT 2016jbu is contentious. The transient is clearly detected at −90 d in VLT + FORS2 imaging. We determine in Section 5.1 that a second eruption (which may represent a genuine CCSN) occurred at ∼−21 d. Using equation (6) from Nadyozhin (2003) and taking the explosion epoch as ∼−90 d, we find a value of $M_{Ni} \leq 0.033$ M$_\odot$, and taking ∼−21 d we find a value of $M_{Ni} \leq 0.016$ M$_\odot$. Following the arguments made in Section 5.1, we will take the latter explosion date as the more plausible, motivated by the apparent second eruption at −21 d (this

Downloaded from https://academic.oup.com/mnras/article/513/4/5666/6581584 by University of Arizona user on 02 September 2022

is the explosion epoch typically assumed in the literature), indicating a potential CCSN.

This limit on ^{56}Ni is consistent with other SN 2009ip-like transients. However, it is clear that during this time there is still ongoing CSM interaction, as demonstrated from the multi-component Hα profile in Paper I, and, as such, this value should be considered a conservative upper limit, assuming any ^{56}Ni is produced at all.

6.2 CSM–ejecta interaction

A previously explored scenario for the double-peaked light curve of SN 2009ip-like objects is that *Event A* represents a low-energy eruption from the progenitor star and *Event B* is powered by the interaction between the ejecta from this eruption and some pre-existing CSM that was ejected in the preceding years (Mauerhan et al. 2013a; Fraser et al. 2013a; Thöne et al. 2017).

We measure the radiated energy released from *Event A* (−90 d to −21 d) as 3.15×10^{47} erg and the energy from *Event B* (−21 d to +450 d) as $\sim 1.81 \times 10^{49}$ erg. Fraser et al. (2013a) find a similar value for SN 2009ip of $\sim 1.8 \times 10^{49}$ erg.

If we assume that *Event A* is a symmetric explosion (similar to that proposed in Mauerhan et al. 2014), we can approximate it using an *Arnett model* (Arnett & Chevalier 1996), taking the diffusion time-scale for a photon to be $t_{\rm d} \approx L^2/D$, where D is a diffusion coefficient, with $D \approx \lambda c = c/(\rho\kappa)$. Assuming that *Event A* corresponds to the adiabatic expansion of a photosphere, and assuming $L \approx R$, we can describe the diffusion time-scale as

$$\tau_{\rm d} = \left(\frac{3\kappa M_{\rm ej}}{4\pi c v_{\rm ej}}\right)^{1/2}, \tag{2}$$

by substituting $R \approx \tau_{\rm d} \times v_{\rm sh}$ and $\rho \approx (3M_{\rm ej})/(4\pi R^3)$, where $M_{\rm ej}$ and $v_{\rm ej}$ are the ejecta mass and velocity, respectively, κ is the opacity of the ejecta, and c is the speed of light. We take the rise time in the r band of *Event A* to be similar to the diffusion time and we obtain a value of ∼60 days. We assume the P Cygni minima follow this dense material ejected prior to, or during, the beginning of *Event A*, as suggested by Thöne et al. (2017) for SN 2015bh. Using equation (2) and taking $v_{\rm ej} \approx 700$ km s^{-1} and assuming a mean opacity of $\kappa = 0.34$ cm^2 g^{-1} (assuming e$^-$ scattering dominates in the H-rich ejecta), we find that $M_{\rm ej}$ for *Event A* is ∼0.35 M$_\odot$, giving a kinetic energy of $\sim 1.7 \times 10^{48}$ erg.

This value is a factor of 10 less than is required to power *Event B*. This is a crude approximation, as we invoke spherical symmetry. To investigate the mass of *Ejecta 1* fully, detailed hydrodynamic simulations are needed (e.g. Vlasis, Dessart & Audit 2016; Suzuki, Moriya & Takiwaki 2019), which are beyond the scope of the work presented here.

Assuming free expansion, the constrained ejection times, and velocities for our multiple-shell models given in Section 5.1, the beginning of *Event B* coincides with material from both shells being at the same location, $R_{\rm BB} \approx 0.7 \times 10^{15}$ cm (Fig. 11). This suggests that *Event B* is powered from the collision at ∼−19 d of *Ejecta 2*, which interacts with the slower moving material ejected at the beginning of *Event A* (*Ejecta 1*).

It is difficult to measure the mass of *Ejecta 2*. If we assume that *Event B* is powered solely by CSM interactions, we calculate that $M_{\rm ej} \sim 0.37$ M$_\odot$ travelling at ∼ 5000 km s^{-1} can account for the energy seen, while allowing for an extremely low porosity (or overlapping surface area between the colliding material) of 10 per cent. This value will change depending on the opening angle of the interaction site, as explored in disc interaction models (Vlasis et al. 2016; Suzuki et al. 2019; Kurfürst, Pejcha & Krtička 2020).

Even with this conservative estimate, our values of $M_{\rm ej}$ are much lower than those seen in CCSNe or η Car. However, extremely low porosity (e.g. 1 per cent) would allow for a few M$_\odot$ of ejected material if we assume no input to the light curve from radioactive decay.

Although observed after peak luminosity, both SN 2013L and SN 2010jl showed a plateau phase after maximum light (Ofek et al. 2014; Taddia et al. 2020). This trend is discussed by Chevalier & Irwin (2011); SN ejecta interacting with a dense mass-loss region can form a plateau in luminosity lasting the duration of the shock interaction and ending when the entire interaction material is shocked. As the photon mean free path increases with the geometric expansion of the CSM, the innermost regions of the interaction are revealed. This was suggested to explain the double-peaked spectral profiles of SN 2010ij (Ofek et al. 2014), SN 2013L (Taddia et al. 2020), and iPTF14hls (Andrews & Smith 2018; Sollerman et al. 2019; Moriya, Mazzali & Pian 2020) at late times. We use the emergence of the blue emission feature and the decrease of the peak velocity offset as a proxy for the shock front. We discuss the evolution of this feature in Paper I. We fit a declining power-law function to the peak velocity of the blue emission from +20 to +120 days, which is fitted well by

$$v_{\rm blue}(t) \approx (1375 \pm 25) \times \left(\frac{t}{100\,{\rm d}}\right)^{-0.40\pm0.03} {\rm km\,s^{-1}}, \tag{3}$$

Both red and blue emission components follow equation (3) well (the red component has a different normalization constant) up until the seasonal gap (+140 days). After that, both components maintain a higher velocity and coast at ∼±1300 km s^{-1} up until the end of our spectroscopic observations (+575 days), see Paper I. Under the assumption of steady-state mass loss, the luminosity from CSM–shock interaction can be described by

$$L_{\rm sh} = \epsilon \frac{1}{2} \frac{\dot{M}}{v_{\rm wind}} v_{\rm ej}^3, \tag{4}$$

where $L_{\rm sh}$ is the luminosity from CSM–ejecta interaction, ϵ is the conversion efficiency from kinetic to thermal energy (taken to be 50 per cent, typical of Type IIn SNe (Smith 2017)), $v_{\rm ej}$ is the ejecta velocity, which is set to equation (3), and $v_{\rm wind}$ is the wind velocity. We fit equation (4) to our bolometric light curve during the period from the *Knee* stage up until the beginning of the seasonal gap. Fitting to this time-frame gives an upper limit for $\dot{M} \approx 0.05$ M$_\odot$ yr^{-1}, if we assume an LBV wind with $v_{\rm wind} \approx 250$ km s^{-1} (we find a similar value for $v_{\rm wind}$ from our earliest Hα profile). Setting $v_{\rm wind} \approx 700$ km s^{-1}, the value of the P Cygni minima, we obtain $\dot{M} \approx 0.14$ M$_\odot$ yr^{-1}.

We base the above calculations on the assumption that the luminosity between +70 d and +140 d is shock–CSM interaction dominated, with no other major contributing energy source, i.e. no major contribution from radioactive decay. If AT 2016jbu is surrounded by a dense, disc-like CSM, the assumption that this phase is interaction-dominated is motivated by models (e.g. fig. 11 from Vlasis et al. 2016). These models show a similar light-curve shape to AT 2016jbu, including a tail resembling radioactive ^{56}Ni decay at ∼ +80 days past maximum brightness (these models assume no ^{56}Ni). Symmetric ejecta and disc interaction models show that the energy input at the *Knee* stage is dominated by this ejecta–disc interaction. We will return to the possibility of disc-like CSM in Section 7.2.

After the seasonal gap (+140 days), the velocity of the red/blue emission does not follow equation (3) and the bolometric luminosity does not follow equation (4). At this point, the light curve has increased in brightness, which is clearly seen in Fig. 12. However by ∼400 d, $L_{\rm bol}$ fades below the value extrapolated from equation (4).

Downloaded from https://academic.oup.com/mnras/article/513/4/5666/6581584 by University of Arizona user on 02 September 2022

After the seasonal gap, both red and blue emission lines have similar FWHM, ∼1500 km s^{-1}, with the red emission having a slightly larger width but converging to the FWHM of the blue component at ∼400 d. If the red/blue emission follows the shock interaction, this suggests an increased velocity of the shock front. Conserving mass flux in the shock, we have $\rho_1 v_1 = \rho_2 v_2$, where subscripts 1,2 represent the post- and pre- shock regions, respectively. If the shock transverses to a lower-density CSM environment, this can account for the increased velocity seen. This might indicate that the shock has now reached a lower-density environment, perhaps created by the series of outbursts in the years prior. However, it is not obvious how interaction with a less dense region of CSM would account for the increased luminosity as well as the increased strength of He I emission lines (also seen in SN 1996al: Benetti et al. 2016) at this time (Paper I).

7 DISCUSSION

In the following section, we will discuss the nature of AT 2016jbu. There is much debate as to the nature of SN 2009ip-like objects (Pastorello et al. 2008, 2019a; Smith & Mauerhan 2012; Fraser et al. 2013a; Graham et al. 2014; Margutti et al. 2014; Smith et al. 2014). Any scenario for AT 2016jbu or SN 2009ip-like transients needs to account for all of the following points:

(1) outbursts reaching an absolute magnitude of $M_r \sim -11 \pm 2$ mag seen in the historic light curve of the transient;
(2) a faint event, reaching an absolute magnitude of $M_r \sim -13 \pm 2$ mag;
(3) a second event a few weeks later, reaching an absolute magnitude of $M_r \sim -18.5 \pm 0.5$ mag and ejecting material with velocities up to $\sim 10\,000$ km s^{-1};
(4) ejected ^{56}Ni mass of $\lesssim 0.02$ M$_\odot$;
(5) no directly observed synthesized material, either from explosive nucleosynthesis or from late-stage stellar evolution.

A possible addition to this list is double-peaked emission lines. This is seen in the majority of SN 2009ip-like transients, although, ironically, not SN 2009ip itself.

We address the probable progenitor in Section 7.1. Using our high-cadence multi-chromatic photometry presented in Paper I and the bolometric evolution from Section 5, we present a likely explosion model and circumstellar (CS) geometry for AT 2016jbu that can be extrapolated to other SN 2009ip-like transients in Section 7.2. We discuss the validity of a CCSN scenario in Sections 7.3 and 7.4, and the possibility of the progenitor being in an interacting binary system in Section 7.5.

7.1 The progenitor of AT 2016jbu and SN 2009ip-like transients

The events of SN 2009ip-like transients may represent a critical step in the late-time evolution of massive stars. A dramatic increase in luminosity allows for super-Eddington winds and high mass-loss rates; however, the mechanism resulting in these outbursts is unknown. Observations of shock features in the Homunculus Nebula around η Car may even point to explosive mass loss. Furthermore, in the classical picture, LBVs should not be SN progenitors, as they have just transitioned to the He-core burning stage in their core.

It is generally thought that SN 2009ip-like transients arise from very massive stars (Foley et al. 2011; Fraser et al. 2013a, 2015; Pastorello et al. 2013, 2019a; Smith et al. 2014; Elias-Rosa et al. 2016; Smith, Andrews & Mauerhan 2016b). The progenitor of SN 2009ip is thought to be a 60–80 M$_\odot$ LBV from pre-explosion images (Smith et al. 2010; Foley et al. 2011). However, this was measured in a single band only, which may be strongly affected by Hα emission. As shown in Fig. 4, the bright contribution of Hα in *F350LP* will provide misleading SED fitting results. While LBVs experience erratic mass loss as they undergo a short transition from O-type to WR stars, AT 2016jbu appears to be too low mass (∼22 M$_\odot$) to be consistent with the SN 2009ip progenitor. We note that this relatively low mass was found while taking into account the effect of Hα emission on the SED.

Our analysis of the progenitor mass for AT 2016jbu is the most secure for any SN 2009ip-like transient in the literature, as it is based on a broad optical to NIR SED, as well as on the local neighbourhood. From our SED fitting to early 2016 *HST* data, we find that the colour of the progenitor is consistent with a yellow hypergiant. Using DUSTY modelling and matching the output spectra to these colour values, we find values for L and T that are consistent with a single-star mass of 22–25 M$_\odot$, consistent with the results from K18. Moreover, the local environment, which can be be assumed to be composed of a similar stellar population, demonstrates that we can effectively rule out a very young population (expected for a 60–80 M$_\odot$ star).

In order to explore the progenitor further, we turn to a grid of stellar models created with the BPASS code. The BPASS stellar model library contains the time-varying properties of over 250 000 star systems for a grid of initial parameters and a population containing a realistic fraction of binary and single star systems (Eldridge et al. 2017; Stanway & Eldridge 2018). Using `hoki`[7] (Stevance et al. 2020a), we searched for models matching the observed temperature and luminosity of the progenitor of AT 2016jbu, considering the possibility of both a terminal core-collapse supernova and a non-terminal event.

For the CCSN (non-terminal explosion) scenario, we find 12 (1668) matching stellar models, and 0 (3) of these models correspond to single star systems.

The zero-age main sequence (ZAMS) and final mass distributions, as well as the evolutionary tracks for both interpretations, are presented in Fig. 13. We can evaluate the mean and standard deviation for the two scenarios: $\overline{\mathrm{M}} = 12.3$ M$_\odot$, $\sigma = 1.9$ M$_\odot$, and $\overline{\mathrm{M}} = 22$ M$_\odot$, $\sigma = 3.4$ M$_\odot$ for CCSN and non-terminal explosion cases, respectively.

We find mean lifetimes of $7.3^{+0.1}_{-.1}$ and $7.0^{+0.1}_{-0.1}$ Myr for the CCSN and non-terminal explosion scenarios, respectively. Very massive stellar progenitors (e.g. classical LBVs with >50 M$_\odot$) are confidently excluded for AT 2016jbu.

There are numerous suggestions in the literature that LBVs can be the direct progenitors of CCSNe (e.g. Trundle et al. 2008; Dwarkadas 2011; Smith & Tombleson 2015; Humphreys et al. 2016; Ustamujic et al. 2021). It has been suggested that the LBV phenomenon may occur in stars with initial masses as low as 20−25 M$_\odot$, particularly when rotation is included in models (Groh, Meynet & Ekström 2013). Such LBVs may appear similar to F-type yellow supergiants during their eruptive stage (Humphreys et al. 2016; Kilpatrick et al. 2018). It is therefore possible that the progenitor of AT 2016jbu is a low-mass LBV. However, we still require a high mass loss of ∼0.05 M$_\odot$ yr^{-1} to explain the light curve of AT 2016jbu. This is not dissimilar to the mass-loss rate of η Car during its Great Eruption (∼0.1 M$_\odot$ yr^{-1}: Davidson & Humphreys 1997), but it remains un-

[7] https://github.com/HeloiseS/hoki

Downloaded from https://academic.oup.com/mnras/article/513/4/5666/6581584 by University of Arizona user on 02 September 2022

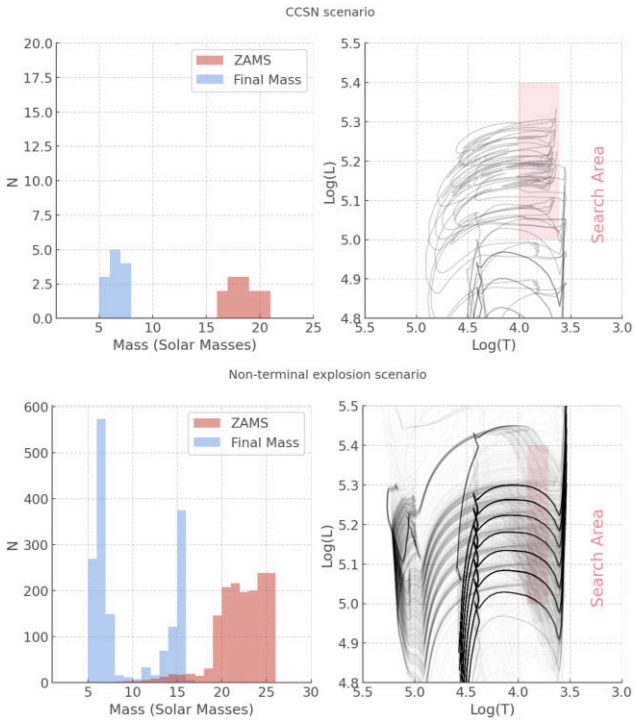

Figure 13. Mass distributions (ZAMS and final) and evolutionary tracks of BPASS models matching the L and T derived from DUSTY modelling. The upper (lower) panel shows the CCSN (non-terminal) scenario. Each evolutionary track is plotted at a low transparency and therefore the lighter the tracks, the rarer they are in our matches. We mark the search area in T and L from Section 2 in each HR diagram.

known whether *lower* mass LBVs can sustain such a high mass-loss rate.

7.2 Geometry of AT 2016jbu and SN 2009ip-like transients

An interesting problem to solve with the CCSN scenario is that of the presence and geometry of the CSM, as discussed in Section 5. The LBV-type winds invoked in Section 6.2 do not apply to lower mass progenitors; indeed we find an average mass-loss rate over the last 1 Myr of $\log(\dot{M}) = -5.4^{+0.2}_{-0.8}$ $M_\odot$ yr^{-1} and $\log(\dot{M}) = -4.9^{+0.2}_{-0.3}$ $M_\odot$ yr^{-1} for the CCSN and non-terminal scenarios, respectively.

One can sustain a dense CSM even with a low mass-loss rate, provided the wind velocity is sufficiently small. Using $\log(\dot{M})/v_{\rm wind}$ as a proxy for wind density, we compare the average ratio found in our models with that assumed in Section 6.2. We find that for both sets of progenitor models $\dot{M}/v_{\rm wind} \approx 10^{-6}$, compared with a value of $\approx 10^{-4}$ found for AT 2016jbu. Thus, we can confidently assert that steady winds are not able to create the CSM observed in AT 2016jbu.

The alternative is episodic mass loss resulting from Roche lobe overflow (RLOF) or common-envelope evolution (CEE). We examined the CCSN progenitor models found in BPASS and find that three models are in a CEE phase at the time of CCSN explosion; furthermore, we find another two undergoing mass transfer. Similarly, for the non-terminal models we find that 937 models are in the CEE phase and 501 are undergoing stable mass transfer at the point where they match the observed L and T of the AT 2016jbu progenitor. Consequently, the BPASS models reveal that the peculiar combination of properties and environment of AT 2016jbu can be explained by binary interactions.

A radially confined, dense, disc-like CS environment has been suggested for SN 2009ip-like transients (Levesque et al. 2014; Margutti et al. 2014; Smith et al. 2014; Fraser et al. 2015; Benetti et al. 2016; Tartaglia et al. 2016a; Andrews & Smith 2018; Pastorello et al. 2018) as well as other Type IIn SNe (van Dyk et al. 1993; Benetti 2000; Stritzinger et al. 2012; Benetti et al. 2016; Andrews et al. 2017; Nyholm et al. 2017) and superluminous supernovae (SLSNe: Metzger 2010; Vlasis et al. 2016).

Double-peaked line profiles are signs of asymmetric environments such as a disc, rings, or bipolar outflows cause by an asymmetric explosion. This is similar to the presence of double-peaked Hα (and other emission lines) originating from accretion discs in active galactic nuclei (e.g. Shapovalova et al. 2004) as well as double-peaked emission from Be/shell stars (e.g. Andrillat, Jaschek & Jaschek 1986), although their formation and powering mechanism are extremely different. We show in Paper I that AT 2016jbu and other SN 2009ip-like objects show a degree of degeneracy in the appearance of their Hα profiles, which may be explained with a simple viewing-angle effect.

We suggest that AT 2016jbu has undergone a series of eruptions, such as has been suggested for η Car (see review by Smith 2009) and SN 2009ip (Levesque et al. 2014; Margutti et al. 2014; Mauerhan et al. 2014; Reilly et al. 2017), and a significant portion, if not all, of the explosion energy is a result of ejecta–ejecta or ejecta–CSM interaction, which dominates around a month after maximum light. It is uncertain whether any of these eruptions emanate from core collapse.

Recently, several groups have modelled the interaction of ejecta with aspherical CSM (Vlasis et al. 2016; McDowell, Duffell & Kasen 2018; Suzuki et al. 2019; Kurfürst et al. 2020; Nagao, Maeda & Ouchi 2020). Vlasis et al. (2016) has modelled the light-curve evolution of a spherically symmetric eject colliding with a disc-like CSM. We find similarities between these models and AT 2016jbu. One important feature is that after $\sim +80$ days these models seem to follow a decay similar to that expected from ^{56}Ni. The energy source at this time is solely powered from CSM interaction and not from radioactive decay. However, these models cannot explain the increased brightness in AT 2016jbu after the seasonal gap, although this likely reflects a clumpy CSM and would require fine-tuning of the CSM density profile.

Models by Kurfürst et al. (2020) have modelled ejecta interaction with aspherical CSM for a range of viewing angles (Model A and fig. 12 in Kurfürst et al. 2020), demonstrating a clear viewing-angle degeneracy, where looking down through the plane of the CSM shows the greatest '*double-peaked*' effect and looking through the material shows the least (i.e singularly peaked emission lines). This can naturally explain the variations in Hα appearance found amongst SN 2009ip-like transients (see Paper I).

For SN 2009ip-like transients, there is some discrepancy as to the eruption epoch of this asymmetric structure, with some authors suggesting this material was ejected close to/during *Event A* (e.g. Margutti et al. 2014; Tartaglia et al. 2016b; Thöne et al. 2017), whereas some authors speculate the disc has been ejected much earlier (e.g. Mauerhan et al. 2013b, 2014). This is difficult to understand without specific stellar evolutionary models.

As discussed in Section 5.1, we proposed a double eruption model, where the first ejecta interacts with pre-existing CSM, followed by a second eruption some months later. The collision of these two ejecta produces the spectral and light-curve evolution we present in Paper I and can be extrapolated to fit the observables of several SN 2009ip-like transients. We provide an illustration in Fig. 14, with a detailed outline of events given in the caption.

Downloaded from https://academic.oup.com/mnras/article/513/4/5666/6581584 by University of Arizona user on 02 September 2022

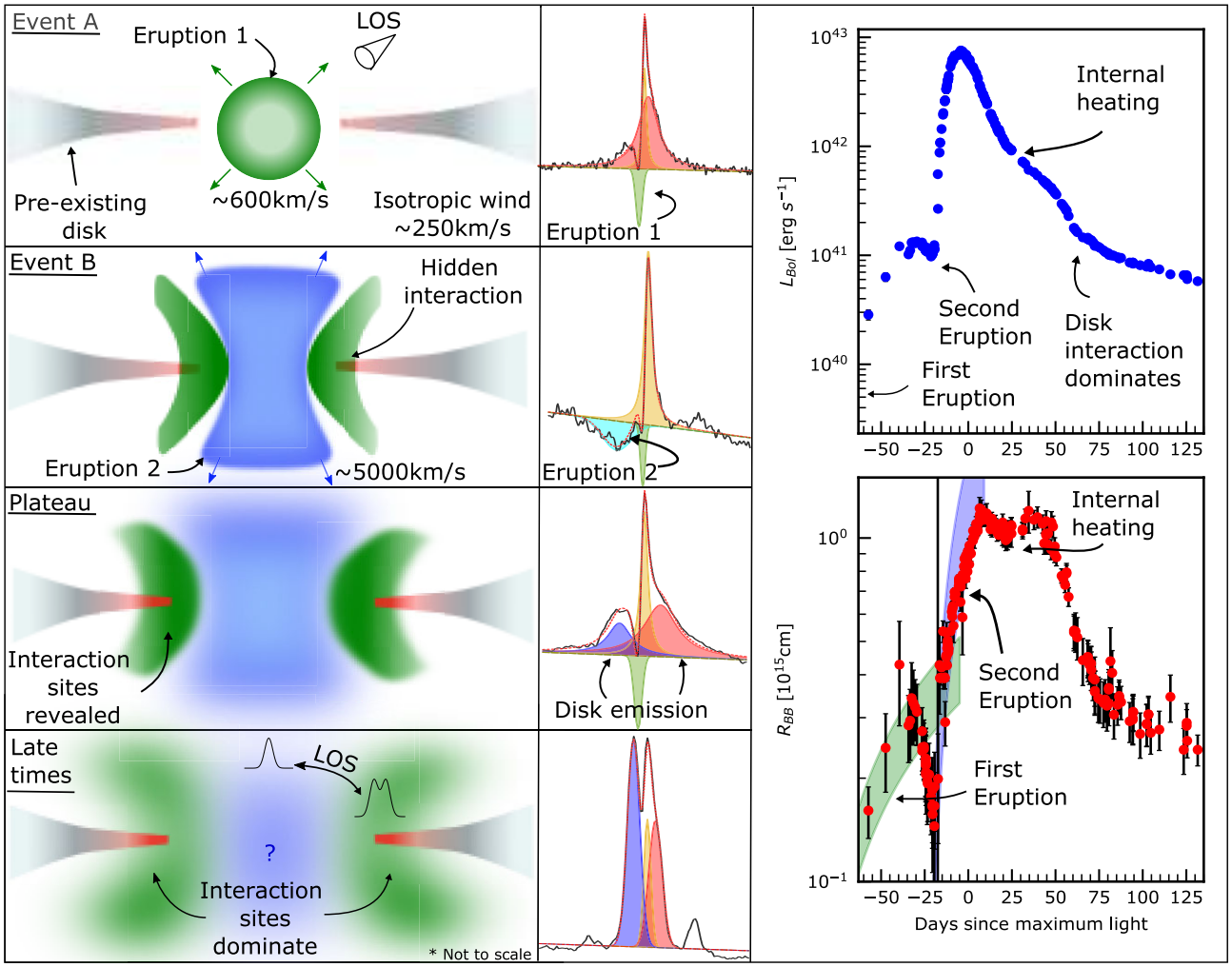

Figure 14. Toy model depicting possible geometry and explosion scenario for AT 2016jbu. This diagram illustrates the discussion in Sections 5.1 and 6.2. The left panels show a simplified illustration of the CS environment around the progenitor at specific epochs. The middle column shows the Hα profile at corresponding epochs. The upper right panel shows the bolometric luminosity and the lower right shows the blackbody radius. We include the distance travelled by *Ejecta 1* (green shaded region) and *Ejecta 2* (blue shaded region). *Event A* begins with an eruption of ejecta 1 which originates from the progenitor system. The eruption and expansion of *Ejecta 1* is seen in $L_{\rm bol}$ and $R_{\rm BB}$, both peaking at ~-27 d. A dense disc-like CSM funnels, and is partially engulfed by, *Ejecta 1*. At ~-21 d, *Ejecta 2* is ejected with a velocity of $\sim$5000 km s^{-1} (this could be the SN explosion) and almost immediately collides with *Ejecta 1* with some fast-moving material escaping along less dense polar regions. $L_{\rm bol}$ and $R_{\rm BB}$ follow the expansion of an opaque *Ejecta 2* following the HV material seen in Hα. *Ejecta 2* becomes optically thin and the photopshere begins to move inwards in velocity space. There is a linear decay in $R_{\rm BB}$ until $\sim+22$ d or the beginning of the plateau stage. $R_{\rm BB}$ plateaus at $\sim+25$ d due to effective internal heating from the site of interaction. Photons originating from the interaction site between *Ejecta 1*, *Ejecta 2*, and the CSM begin to diffuse outwards, as the material becomes partially transparent. This coincides with the metamorphosis of the blue HV absorption to an emission profile. At $\sim+45$ d, the *Knee* stage drops in $L_{\rm bol}$ and $R_{\rm BB}$, with $R_{\rm BB}$ at a slightly higher value compared with the beginning of *Event B*. Both red and blue emission lines narrow at this stage, which may signify that any intervening material is now completely optically thin and any escaping photons undergo minimal scattering. The dominant source of energy is now shock interaction due to ejecta–CSM interaction. In the bottom left panel we also include a line-of-sight dependence. We expect the transient to show double-peaked emission lines when observed near the equator (e.g. AT 2016jbu, SN 2015bh, SN 1996al) and more singularly peaked lines when observed towards the polar regions (e.g. SN 2009ip). We note the similarities between this toy model and those proposed for η Car (e.g. Smith et al. 2018).

7.3 Modelling the light curve using SNEC

To explore further the plausibility of the progenitor matching BPASS models from Section 7.1, we exploded a small subset of these with the SuperNova Explosion Code (SNEC: Morozova et al. 2015). The full details of how BPASS models are exported and exploded within SNEC can be found in Eldridge et al. (2019). The key addition to using the progenitor model structure is to add on a CSM component around the star. Here we use the values derived in Section 5.1, a terminal wind velocity of 250 km s^{-1}, and a mass-loss rate of 0.05 M$_\odot$ yr^{-1}. For each of the input stellar models we use an explosion energy of 5.6 $\times$ 10^{49} erg, 0.016 M$_\odot$ of ^{56}Ni, and an inner mass cut at 5 M$_\odot$ with nickel mixing out to 0.6 M$_\odot$. The resultant simulated bolometric light curves are shown in Fig. 15 and the model parameters are given in Table 2.

Our models are able to reproduce the magnitude of the peak luminosity, although exact matching of the light curve post-peak is difficult. Phases of the swept-up wind becoming transparent, followed by the ejecta, can be seen as sudden drop-offs in Fig. 15. We find that the width of the *Event B* peak is dependent to some degree

Downloaded from https://academic.oup.com/mnras/article/513/4/5666/6581584 by University of Arizona user on 02 September 2022

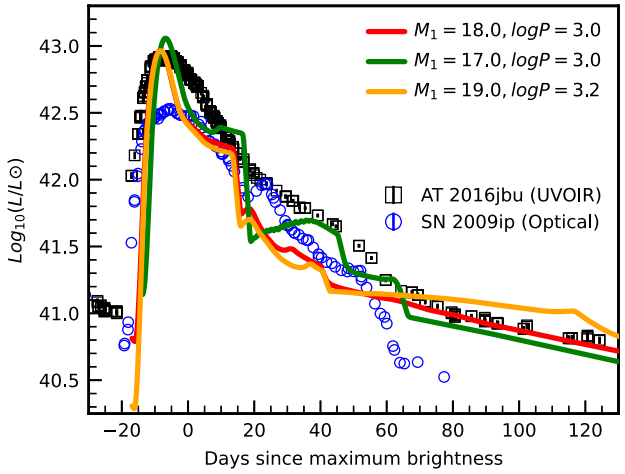

Figure 15. Diagram showing the observed light curve and light curves simulated by SNEC from progenitors that match the pre-explosion constraints. All include the circumstellar medium as described earlier. We include our pseudo-bolometric light curve for AT 2016jbu in black and the optical pseudo-bolometric light curve for SN 2009ip in blue (Fraser et al. 2013b; Pastorello et al. 2013).

Table 2. The parameters of the BPASS models exploded with SNEC.

M_1 /$M_\odot$	M_2 /$M_\odot$	log (P_i/days)	M_{final} /$M_\odot$	M_{CO} /$M_\odot$
17	11.9	3	5.9	4.0
18	16.2	3	6.5	4.1
19	13.3	3.2	7.2	5.4

on how the density of the wind varies with distance from the star. The figure shows the resultant models, where we assume $\rho_{wind}(r) \propto r^{-1.6}$. We found that the shallower the density gradient, the wider the peak, and a best match is found with an exponent $n = -1.6$. In general, the models that match the supernova light curve best have low ejecta masses of the order of 1–2 $M_\odot$. Some models that have experienced a merger during their binary evolution and have a higher ejecta mass do not match the light curve, being less luminous or evolving more slowly. Achieving an exact match between the models and observed light curve would require significant fine-tuning of the details of the CSM around the star, in terms of density profile, wind velocity, and details of the wind acceleration. An exact match may also be impossible given the spherically symmetric assumptions of SNEC. However, we take the reasonably close match between the model and observed light curves to indicate that a subset of the BPASS models can explain AT 2016jbu.

Intriguingly, the low CO core mass of several of the progenitor models suggests an explosion close to the electron-capture regime, where lower nickel masses and explosion energies would be expected.

7.4 Was AT 2016jbu a core-collapse supernova?

The main point of controversy is whether AT 2016jbu and SN 2009ip-like transients are indeed CCSNe, meaning the progenitor has been destroyed and the transient will eventually decay following a radioactive decay tail. This begs the question: if these are indeed CCSNe, *when did core-collapse occur?*

SN 2009ip-like transients display two broad, luminous events, rather than the singularly peaked light curve typically associated with SNe. Mauerhan et al. (2013b) suggest that *Event A* is a CCSN and *Event B* is a result of ejecta interacting with dense CSM. In this scenario, with respect to AT 2016jbu, the duration of *Event A* ($\sim$ 60 days) is the time needed for this ejecta to reach the inner edge of the CSM. This scenario would be consistent with the early evolution of R_{BB} expanding at $\sim$700 km s^{-1}; however, this velocity is implausibly slow for SN ejecta. More problematic still, at -21 d we see an increase in velocity where R_{BB} expands at $\sim$4500 km s^{-1}. In the case of core collapse, we hence regard it as more plausible that *Event B* is the terminal explosion of the progenitor, where the ejecta interacts with a non-terminal outburst that was ejected at $\sim$700 km s^{-1} around the start of *Event A*. This scenario is also reinforced by the rise time ($\sim$17 days) and peak magnitude ($M_V \sim -18.5$ mag) of *Event B* (Nyholm et al. 2020).

We find a low value of ^{56}Ni of $\lesssim 0.016$ $M_\odot$ for AT 2016jbu, consistent with other SN 2009ip-like transients. Such a low ^{56}Ni mass would be unusual for a normal CCSN, although an exception would be a faint electron-capture SN (ECSN) or a subluminous Fe CCSN from a star with a ZAMS mass of around 8–10 $M_\odot$. However, we find the mass of the AT 2016jbu progenitor to be significantly larger than that expected for an ECSN progenitor (Doherty et al. 2017). Additionally, the inferred explosion energy of 5.6×10^{50} erg (which may be a lower limit, as spherical symmetry is assumed) is too high for a typical ECSN (Wanajo et al. 2009). A final possibility that can explain such a low Ni mass (if this is a CCSN) is significant fallback on to a compact remnant (Zampieri, Shapiro & Colpi 1998; Benetti et al. 2016).

Some challenges remain for the fallback scenario. A low-metallicity environment is required, so that the progenitor star has retained much of its ZAMS mass (e.g. Heger et al. 2003). This is hence an appealing scenario for SN 2009ip, due to its remote location ($\sim$5 kpc from its host: Smith et al. 2016b) and naturally low-metallicity environment. Conversely, this contradicts what we see for the environment around AT 2016jbu in Section 4.2, where we find an approximate solar metallicity of 8.66 dex. It is hence expected that a $\sim$20-$M_\odot$ progenitor will lose a significant fraction of its mass before exploding.

We see from Fig. 9 that AT 2016jbu is located near a moderately star-forming region that is likely to host CCSNe, as seen from SN 1999ga. In contrast, SN 2009ip is located on the outskirts of its host spiral galaxy, NGC 7259, at a galactocentric radius of $\sim$ 5 kpc. Smith et al. (2016b) find no strong indication of massive star formation anywhere in the vicinity around SN 2009ip, unlike what is seen for AT 2016jbu. If the progenitors of SN 2009ip and AT 2016jbu are similar, as is suggested by their photometric and spectral evolution, then this begs the question of why SN 2009ip is on its own.

One of the biggest difficulties with AT 2016jbu as a CCSN is that it is in stark contrast to the predictions of single-star stellar evolutionary models. A 20-$M_\odot$ star is expected to end its life as an RSG that undergoes Fe core collapse (Heger et al. 2003). From our DUSTY modelling in Section 2, we find that the progenitor of AT 2016jbu is not situated at the end of any single-star evolutionary track. This suggests that the progenitor is not sufficiently evolved to undergo core collapse. Our conclusion in Section 2 also suggests that the progenitor of AT 2016jbu is not an RSG but rather a YHG. We also note that, if AT 2016jbu is indeed a CCSN, it is more appropriate to compare the luminosity of the progenitor with the *terminal luminosity* of the models (typically corresponding to the end of core He-burning), in which case we find that it must have been a 12–16 $M_\odot$ star. One must caution, however, that if the progenitor of AT 2016jbu was in a binary, then the expectations from single-

Downloaded from https://academic.oup.com/mnras/article/513/4/5666/6581584 by University of Arizona user on 02 September 2022

star evolution can be drastically altered. However, even if AT 2016jbu does arise from a binary progenitor system, models do not necessarily predict outbursts or eruptions immediately prior to explosion, as seen in this case (discussed further in Section 7.5 below). Clearly, further detailed stellar evolutionary modelling is required to explain the progenitor (or progenitor system) of AT 2016jbu fully.

A tantalizing hint of a surviving progenitor is AT 2016jbu returning to its pre-explosion magnitude in 2019, as shown in Fig. 2. However, this detection may be serendipitous and further late-time monitoring will be needed to confirm any surviving progenitor.

7.5 Binary interaction

Several authors have suggested that SN 2009ip-like transients are a result of binary interaction (Smith et al. 2014, 2018; Kashi et al. 2013; Soker & Kashi 2013), as well as those of some other SN impostors, e.g. SN 2000ch (Pastorello et al. 2010; Smith 2011; Clark et al. 2013). Mass transfer within a binary system could naturally explain an asymmetric CSM environment, which we interpret as a circumstellar/circumbinary disc for AT 2016jbu.

Smith & Tombleson (2015) suggest that the isolated location of SN 2009ip may be explained, as they are *Kicked Mass Gainers* in a binary star system. For the progenitor to travel $\sim$ 5 kpc within the required lifespan of a 50–80 $M_{\odot}$ star, a binary companion may be required to provide an additional source of fuel after the stars have been ejected (Smith et al. 2016b).

Binary merger events have recently been associated with red novae (RNe) and the more extreme luminous red novae (LRNe) (see review by Pastorello et al. 2019b, and references therein). These transients typically fall into the class of gap transients (Kasliwal et al. 2012; Pastorello & Fraser 2019) and are amongst the most powerful stellar cataclysms. LRNe span a wide range of absolute magnitudes, from -4 to -15 mag (Pastorello & Fraser 2019), and show a wide range of light-curve shapes and durations.

The physical interpretation of LRNe is debated. The progenitors of LRNe are likely massive contact binaries, and the double-peaked light curve is a consequence of a stellar merger plus common-envelope ejection (CEE: Smith et al. 2016a; Metzger & Pejcha 2017; Pastorello et al. 2019b). Pastorello et al. (2019b) suggest that there may be a continuum spanning from RNe to LRNe, with the possibility that this range can reach to brighter magnitudes (most likely caused by higher mass systems). SN 2009ip-like events may be some combination of binary merger where the system consists of a relatively massive primary, where the stars undergo a common-envelope (CE) phase followed by a massive eruption.

AT 2016jbu and SN 2009ip-like transients show a common peak magnitude and shape (i.e. *Event B* appears to be similar among SN 2009ip-like events). We do not have adequate colour information for the peak of *Event A* for AT 2016jbu; however, *Event B* has a colour of $B - V \sim 0$, which is comparable with that seen in LRNe in their first peak. AT 2016jbu never gets redder than $B - V \lesssim 0.8$, and after $\sim$ 1.2 years the transient returns to a $B - V$ value of $\sim$ 0.2. If AT 2016jbu is indeed related to LRNe, continued interaction in AT 2016jbu may be responsible for the relatively blue colour at late times.

Soker & Kashi (2013) proposed that SN 2009ip is the result of the merger of a massive LBV with a binary companion in their 'mergerburst' model. This model agrees quite well with observations of SN 2009ip, such as the moderate ejecta mass (a few $M_{\odot}$), most of which is moving at less than 5000 km s^{-1}. They further predict that the remnant of their mergerburst will be a hot red giant star, which will become apparent years after the transient fades, as is commonly associated with RNe and LRNe (e.g Pastorello et al. 2019b). Kashi et al. (2013) discuss an explosion mechanism similar to the scenario we discuss in Section 5.1 and conclude that the double-peaked light curve of SN 2009ip may be explained by two successive outbursts, separated by $\sim$20 days, caused by periastron passages of the binary system.

It is appealing to conclude that AT 2016jbu is the result of a coalescing binary. This can naturally explain the historic variability, double-peaked light curve, and (inferred) asymmetric CS environment, i.e. disc or bipolar outflow. Metzger & Pejcha (2017) proposed that LRNe can be modelled well by a single symmetric eruption in an asymmetric CSM environment. This asymmetric CSM is fuelled by mass transfer within the binary over many orbits preceding the double-peaked event. The first peak of LRNe can be comfortably powered via cooling envelope emission from fast-moving ejecta. Radiative shocks from the collision of this ejecta with material in the equatorial plane then power the second peak. This would be inconsistent with our proposed '*catch-up*' scenario for AT 2016jbu, although it cannot be ruled out conclusively.

We can speculate that the events prior to *Event B* in AT 2016jbu and SN 2009ip-like events are similar to LRNe, including the mass transfer/Roche lobe overflow (RLOF) seen in the decade leading up to *Event A*, and a merger/CEE powering *Event A* itself. To explain the homogeneity of *Event B*, the merging of the binary system must cause a violent (and possibly terminal) eruption.

Each SN 2009ip-like transient remains relatively blue for a long period of time, unlike what we see in LRNe, which is likely a sign of continued interaction. If we assume that SN 2009ip-like transients are indeed an upscaled version of LRNe, then this continued interaction at late times may reflect a more massive progenitor than is commonly associated with LRNe. In this scenario, we would expect a surviving star to become visible after this interaction has abated.

8 CONCLUSION

In this work, we have investigated the progenitor and environment of AT 2016jbu as well as modelling the transient itself. If AT 2016jbu is a single star, we find that the progenitor is consistent with a $\sim$ 22-$M_{\odot}$ progenitor (e.g. fig. 4 in Smartt et al. 2009), with a colour consistent with a YHG, roughly consistent with K18. Modelling of circumstellar dust using DUSTY gives a luminosity and temperature of the progenitor similar to known YHGs. We show that the local environment around the progenitor of AT 2016jbu is consistent with a CCSN from a progenitor with ZAMS mass $\sim$ 20 $M_{\odot}$, as the stellar population has an age of 15–200 Myr. We confidently rule out the possibility that the progenitor of AT 2016jbu is an LBV of 50–80 $M_{\odot}$, as has been proposed for SN 2009ip (Smith et al. 2010; Foley et al. 2011).

We find that the *Event A/B* light curve can be modelled by two shells of material, with the later *Event B* being powered by a 'catch-up' scenario, involving two eruptive mass-loss events and pre-existing CSM. Spectroscopic and photometric evolution is consistent with spherically symmetric ejecta colliding with, and temporarily engulfing, previously ejected, asymmetric material. This interaction is the dominant energy source after $\sim$ 2 months. After $\sim$ 200 days, AT 2016jbu shows increased interaction, likely reflecting a clumpy CSM.

AT 2016jbu shows tentative evidence for core collapse. We find an upper limit of ^{56}Ni of $\lesssim 0.016$ $M_{\odot}$, but with strong ongoing CSM interaction at this time, the real value of ^{56}Ni is probably much lower (if any at all). Almost 1.5 years after maximum brightness, AT 2016jbu lacks signs of explosively nucleosynthesized material or emission from the burning products of late-time stellar evolution.

Downloaded from https://academic.oup.com/mnras/article/513/4/5666/6581584 by University of Arizona user on 02 September 2022

We explore the possibility that AT 2016jbu is the result of a binary system. We compare our progenitor models with an extensive group of BPASS models, exploring both CCSN and non-terminal events. We find that matching models have $M_{\rm ZAMS} \lesssim 26$ M$_\odot$. Steady-state mass loss due to the progenitor wind is unable to produce the CSM density necessary to power the light curve and episodic mass loss may be required. Using SNEC, we find that a relatively low explosion energy (5.5×10^{49} erg) with a small ejecta mass ($\sim$ 1–2 M$_\odot$) can comfortably power AT 2016jbu (assuming spherical symmetry). If we account for a high degree of asymmetry, we may have an explosion energy on par with a typical CCSN.

It appears that there is not a simple explanation for these transients. Following *Hickam's dictum*, a low-energy SN within a binary system with a disc-like CSM can account for the rise and peak of *Event B*, low ^{56}Ni, continued CSM interaction, and unique spectral features of AT 2016jbu. Additional binary interaction might explain *Event A*, due e.g. to a merger or CEE. Detailed modelling of this proposed scenario is beyond the scope of this article and future work will involve exploring these scenarios in a non-symmetric setting.

The true nature of AT 2016jbu (and other SN 2009ip-like transients) remains elusive. Perhaps the ultimate answer will come if or when very-late-time observations reveal a surviving progenitor. To date, no conclusive evidence exists as to whether these transients destroy their progenitor. However, one must account for the possibility that, if the progenitor survived, it may be obscured by a significant amount of dust. Deep images covering the full SED will hence be required to confidently rule out a surviving, but dust-enshrouded, star. To this end, future observations with the upcoming *James Webb Space Telescope* will be essential. Alongside this, deep optical imaging from the Vera C. Rubin Observatory may capture similar pre-explosion variability in the years/decades prior to future SN 2009ip-like events, perhaps even allowing for a countdown timer before these events.

ACKNOWLEDGEMENTS

SJB acknowledges support from Science Foundation Ireland and the Royal Society (RS-EA/3471). MF is supported by a Royal Society–Science Foundation Ireland University Research Fellowship. TMB was funded by CONICYT PFCHA/DOCTORADOBECAS CHILE/2017-72180113 and acknowledges financial support from the Spanish Ministerio de Ciencia e Innovación (MCIN), the Agencia Estatal de Investigación (AEI) 10.13039/501100011033 under the PID2020-115253GA-I00 HOSTFLOWS project, and Centro Superior de Investigaciones Científicas (CSIC) under the PIE project 20215AT016. KM is funded by the EU H2020 ERC grant no. 758638. TWC acknowledges EU Funding under Marie Skłodowska–Curie grant H2020-MSCA-IF-2018-842471, and thanks Thomas Krühler for GROND data reduction. MN is supported by a Royal Astronomical Society Research Fellowship. BJS is supported by NSF grants AST-1908952, AST-1920392, AST-1911074, and NASA award 80NSSC19K1717. MS is supported by generous grants from Villum FONDEN (13261,28021) and by a project grant (8021-00170B) from the Independent Research Fund Denmark. LH acknowledges support for Watcher from Science Foundation Ireland grant 07/RFP/PHYF295. Time-domain research by DJS is supported by NSF grants AST-1821987, 1813466, and 1908972, and by the Heising–Simons Foundation under grant #2020-1864. NER acknowledges support from MIUR, PRIN 2017 (grant 20179ZF5KS). Support for JLP is provided in part by ANID through the Fondecyt regular grant 1191038 and through the Millennium Science Initiative grant ICN12_009, awarded to The Millennium Institute of Astrophysics, MAS. LG acknowledges financial support from the Spanish Ministry of Science, Innovation and Universities (MICIU) under the 2019 Ramón y Cajal program RYC2019-027683 and from the Spanish MICIU project PID2020-115253GA-I00. DAH and DH are supported by AST-1911151, AST19-11225, and NASA Swift grant 80NSSC19K1639. GP acknowledges support by the Ministry of Economy, Development, and Tourism's Millennium Science Initiative through grant IC120009, awarded to The Millennium Institute of Astrophysics, MAS. LT acknowledges support from MIUR (PRIN 2017 grant 20179ZF5KS). Support for TW-SH was provided by NASA through the NASA Hubble Fellowship grant *HST*-HF2-51458.001-A awarded by the Space Telescope Science Institute, which is operated by the Association of Universities for Research in Astronomy, Inc., for NASA, under contract NAS5-26555. HK was funded by the Academy of Finland projects 324504 and 328898.

This research made use of ASTROPY,[8] a community-developed core PYTHON package for Astronomy (Astropy Collaboration 2013; Price-Whelan et al. 2018). This research made use of data provided by Astrometry.net.[9] Parts of this research were supported by the Australian Research Council Centre of Excellence for All Sky Astrophysics in Three Dimensions (ASTRO 3D), through project number CE170100013. This research has made use of the NASA/IPAC Extragalactic Database (NED), which is operated by the Jet Propulsion Laboratory, California Institute of Technology, under contract with the National Aeronautics and Space Administration. We acknowledge the Telescope Access Program (TAP) funded by the NAOC, CAS, and the Special Fund for Astronomy from the Ministry of Finance. This work was partially supported by Polish NCN grants: Harmonia No. 2018/30/M/ST9/00311 and Daina No. 2017/27/L/ST9/03221. This work made use of v2.2.1 of the Binary Population and Spectral Synthesis (BPASS) models as described in Eldridge et al. (2017) and Stanway & Eldridge (2018). This research is based on observations made with the NASA/ESA *Hubble Space Telescope* obtained from the Space Telescope Science Institute, which is operated by the Association of Universities for Research in Astronomy, Inc., under NASA contract NAS 5-26555. These observations are associated with program 15645. Observations were also obtained from the Hubble Legacy Archive, which is a collaboration between the Space Telescope Science Institute (STScI/NASA), the Space Telescope European Coordinating Facility (ST-ECF/ESAC/ESA), and the Canadian Astronomy Data Centre (CADC/NRC/CSA). This research has made use of the SVO Filter Profile Service[10] supported from the Spanish MINECO through grant AYA2017-84089.

DATA AVAILABILITY

The photometric and spectroscopic data underlying this article are available as described in Paper I. The BPASS models are available at https://bpass.auckland.ac.nz/, while *HST* data are available at the Mikulski Archive for Space Telescopes at https://archive.stsci.edu.

REFERENCES

Anderson J. P., 2019, A&A, 628, A7
Andrews J. E., Smith N., 2018, MNRAS, 477, 74

[8] http://www.astropy.org
[9] https://astrometry.net/use.html
[10] http://svo2.cab.inta-csic.es/theory/fps/

Downloaded from https://academic.oup.com/mnras/article/513/4/5666/6581584 by University of Arizona user on 02 September 2022

Andrews J. E., Smith N., McCully C., Fox O. D., Valenti S., Howell D. A., 2017, MNRAS, 471, 4047
Andrillat Y., Jaschek M., Jaschek C., 1986, A&AS, 65, 1
Arnett D., Chevalier R., 1996, Supernovae and Nucleosynthesis: An Investigation of the History of Matter, from the Big Bang to the Present, Princeton Univ. Press., Princeton
Astropy Collaboration, 2013, A&A, 558, A33
Benetti S., 2000, Mem. Soc. Astron. Italiana, 71, 323
Benetti S. et al., 2016, MNRAS, 456, 3296
Boian I., Groh J. H., 2018, A&A, 617, A115
Botticella M. T., Smartt S. J., Kennicutt R. C. J., Cappellaro E., Sereno M., Lee J. C., 2012, Mem. Soc. Astron. Italiana Suppl., 19, 158
Brennan S. J. et al., 2021, preprint (arxiv:2102.09576)
Bressan A., Marigo P., Girardi L., Salasnich B., Dal Cero C., Rubele S., Nanni A., 2012, MNRAS, 427, 127
Cardelli J. A., Clayton G. C., Mathis J. S., 1989, ApJ, 345, 245
Chen Y., Bressan A., Girardi L., Marigo P., Kong X., Lanza A., 2015, MNRAS, 452, 1068
Chevalier R. A., Irwin C. M., 2011, ApJ, 729, L6
Clark J. S., Bartlett E. S., Coe M. J., Dorda R., Haberl F., Lamb J. B., Negueruela I., Udalski A., 2013, A&A, 560, A10
Davidson K., Humphreys R. M., 1997, ARA&A, 35, 1
de Jager C., 1998, A&A Rev., 8, 145
Doherty C. L., Gil-Pons P., Siess L., Lattanzio J. C., 2017, PASA, 34, e056
Dolphin A. E., 2000, PASP, 112, 1383
Domínguez A. et al., 2013, ApJ, 763, 145
Dopita M. A., Kewley L. J., Sutherland R. S., Nicholls D. C., 2016, Ap&SS, 361, 61
Drilling J. S., Landolt A. U., 2000, in Cox A. N., ed., Allen's Astrophysical Quantities. Springer-Verlag, New York, p. 381
Dwarkadas V. V., 2011, MNRAS, 412, 1639
Eldridge J. J., Stanway E. R., Xiao L., McClelland L. A. S., Taylor G., Ng M., Greis S. M. L., Bray J. C., 2017, PASA, 34, e058
Eldridge J. J., Guo N. Y., Rodrigues N., Stanway E. R., Xiao L., 2019, PASA, 36, e041
Elias-Rosa N. et al., 2016, MNRAS, 463, 3894
Foley R. J., Berger E., Fox O., Levesque E. M., Challis P. J., Ivans I. I., Rhoads J. E., Soderberg A. M., 2011, ApJ, 732, 32
Fraser M., 2020, Royal Soc. Open Sci., 7,200467
Fraser M. et al., 2013a, MNRAS, 433, 1312
Fraser M. et al., 2013b, ApJ, 779, L8
Fraser M. et al., 2015, MNRAS, 453, 3886
Fukugita M., Ichikawa T., Gunn J. E., Doi M., Shimasaku K., Schneider D. P., 1996, AJ, 111, 1748
Galbany L. et al., 2016, MNRAS, 455, 4087
Gogarten S. M., Dalcanton J. J., Murphy J. W., Williams B. F., Gilbert K., Dolphin A., 2009, ApJ, 703, 300
Graham M. L. et al., 2014, ApJ, 787, 163
Graham M. L. et al., 2017, MNRAS, 469, 1559
Groh J. H., Meynet G., Ekström S., 2013, A&A, 550, L7
Gustafsson B., Edvardsson B., Eriksson K., Jørgensen U. G., Nordlund Å., Plez B., 2008, A&A, 486, 951
Heger A., Fryer C. L., Woosley S. E., Langer N., Hartmann D. H., 2003, ApJ, 591, 288
Humphreys R. M., Weis K., Davidson K., Gordon M. S., 2016, ApJ, 825, 64
Husser T. O., Wende-von Berg S., Dreizler S., Homeier D., Reiners A., Barman T., Hauschildt P. H., 2013, A&A, 553, A6
Ivezic Z., Elitzur M., 1997, MNRAS, 287, 799
Kashi A., Soker N., Moskovitz N., 2013, MNRAS, 436, 2484
Kasliwal M. M. et al., 2012, ApJ, 755, 161
Kennicutt Robert C. J., 1998, ARA&A, 36, 189
Kiewe M. et al., 2012, ApJ, 744, 10
Kilpatrick C. D. et al., 2018, MNRAS, 473, 4805 (K18)
Klochkova V. G., Chentsov E. L., Miroshnichenko A. S., Panchuk V. E., Yushkin M. V., 2016, MNRAS, 459, 4183
Kuncarayakti H. et al., 2020, ApJ, 902, 139
Kurfürst P., Pejcha O., Krtička J., 2020, A&A, 642, A214
Levesque E. M., Stringfellow G. S., Ginsburg A. G., Bally J., Keeney B. A., 2014, AJ, 147, 23
Lim P. L., 2020, synphot v1.0.1, Zenodo, available at 10.5281/zenodo.3971036
Maeder A., Meynet G., 2000, ARA&A, 38, 143
Marchant P., Renzo M., Farmer R., Pappas K. M. W., Taam R. E., de Mink S. E., Kalogera V., 2019, ApJ, 882, 36
Margutti R. et al., 2014, ApJ, 780, 21
Marigo P. et al., 2017, ApJ, 835, 77
Mauerhan J. C. et al., 2013a, MNRAS, 430, 1801
Mauerhan J. C. et al., 2013b, MNRAS, 431, 2599
Mauerhan J. et al., 2014, MNRAS, 442, 1166
Maund J. R., 2017, MNRAS, 469, 2202
McCall M. L., 2004, AJ, 128, 2144
McDowell A. T., Duffell P. C., Kasen D., 2018, ApJ, 856, 29
Meikle W. P. S. et al., 2007, ApJ, 665, 608
Metzger B. D., 2010, MNRAS, 409, 284
Metzger B. D., Pejcha O., 2017, MNRAS, 471, 3200
Mihos J. C., Bothun G. D., 1997, ApJ, 481, 741
Moriya T. J., Mazzali P. A., Pian E., 2020, MNRAS, 491, 1384
Morozova V., Piro A. L., Renzo M., Ott C. D., Clausen D., Couch S. M., Ellis J., Roberts L. F., 2015, ApJ, 814, 63
Nadyozhin D. K., 2003, MNRAS, 346, 97
Nagao T., Maeda K., Ouchi R., 2020, MNRAS, 497, 5395
Nicholl M., 2018, Research Notes of the American Astronomical Society, 2, 230
Nyholm A. et al., 2017, A&A, 605, A6
Nyholm A. et al., 2020, A&A, 637, A73
Ofek E. O. et al., 2014, ApJ, 781, 42
Pancoast A., Sajina A., Lacy M., Noriega-Crespo A., Rho J., 2010, ApJ, 723, 530
Pastorello A., Fraser M., 2019, Nature Astronomy, 3, 676
Pastorello A. et al., 2008, MNRAS, 389, 113
Pastorello A. et al., 2009, A&A, 500, 1013
Pastorello A. et al., 2010, MNRAS, 408, 181
Pastorello A. et al., 2013, ApJ, 767, 1
Pastorello A. et al., 2018, MNRAS, 474, 197
Pastorello A. et al., 2019a, A&A, 628, A93
Pastorello A. et al., 2019b, A&A, 630, A75
Price-Whelan A. M. et al., 2018, AJ, 156, 123
Prieto J. L. et al., 2014, ApJ, 787, L8
Reguitti A. et al., 2019, MNRAS, 482, 2750
Reilly E., Maund J. R., Baade D., Wheeler J. C., Höflich P., Spyromilio J., Patat F., Wang L., 2017, MNRAS, 470, 1491
Ryder S. D. et al., 2001, ApJ, 555, 232
Schlafly E. F., Finkbeiner D. P., 2011, ApJ, 737, 103
Shapovalova A. I. et al., 2004, A&A, 422, 925
Smartt S. J., Eldridge J. J., Crockett R. M., Maund J. R., 2009, MNRAS, 395, 1409
Smith N., 2009, preprint (arXiv:0906.2204)
Smith N., 2011, MNRAS, 415, 2020
Smith N., 2017, Handbook of Supernovae, 29, 403
Smith N., Mauerhan J., 2012, The Astronomer's Telegram, 4412, 1
Smith N., Tombleson R., 2015, MNRAS, 447, 598
Smith N., Foley R. J., Filippenko A. V., 2008, ApJ, 680, 568
Smith N. et al., 2010, AJ, 139, 1451
Smith N., Mauerhan J. C., Kasliwal M. M., Burgasser A. J., 2013, MNRAS, 434, 2721
Smith N., Mauerhan J. C., Prieto J. L., 2014, MNRAS, 438, 1191
Smith N., Andrews J. E., Mauerhan J. C., Zheng W., Filippenko A. V., Graham M. L., Milne P., 2015, MNRAS, 455, 3546
Smith N. et al., 2016a, MNRAS, 458, 950
Smith N., Andrews J. E., Mauerhan J. C., 2016b, MNRAS, 463, 2904
Smith N. et al., 2018, MNRAS, 480, 1466
Soker N., Kashi A., 2013, ApJ, 764, L6
Sollerman J. et al., 2019, A&A, 621, A30
Stanway E. R., Eldridge J. J., 2018, MNRAS, 479, 75

Downloaded from https://academic.oup.com/mnras/article/513/4/5666/6581584 by University of Arizona user on 02 September 2022

Stevance H., Eldridge J., Stanway E., 2020a, J. Open Source Softw., 5, 1987
Stevance H. F., Eldridge J. J., McLeod A., Stanway E. R., Chrimes A. A., 2020b, MNRAS, 498, 1347
Stritzinger M. et al., 2012, ApJ, 756, 173
Suzuki A., Moriya T. J., Takiwaki T., 2019, ApJ, 887, 249
Taddia F. et al., 2015, A&A, 580, A131
Taddia F. et al., 2020, A&A, 638, A92
Tartaglia L. et al., 2016a, MNRAS, 459, 1039
Tartaglia L. et al., 2016b, ApJ, 823, L23
Thöne C. C. et al., 2017, A&A, 599, A129
Tonry J. L. et al., 2018, PASP, 130, 064505
Trundle C., Kotak R., Vink J. S., Meikle W. P. S., 2008, A&A, 483, L47
Ustamujic S. et al., 2021, A&A, 654, 167
Vale Asari N. et al., 2020, MNRAS, 498, 4205
van Dyk S. D., Weiler K. W., Sramek R. A., Panagia N., 1993, ApJ, 419, L69
Vlasis A., Dessart L., Audit E., 2016, MNRAS, 458, 1253
Wanajo S., Nomoto K., Janka H. T., Kitaura F. S., Müller B., 2009, ApJ, 695, 208
Whitmore B. C. et al., 2016, AJ, 151, 134
Williams B. F., Hillis T. J., Murphy J. W., Gilbert K., Dalcanton J. J., Dolphin A. E., 2018, ApJ, 860, 39
Wong O. I. et al., 2006, MNRAS, 371, 1855
Woosley S. E., Blinnikov S., Heger A., 2007, Nature, 450, 390
Zampieri L., Shapiro S. L., Colpi M., 1998, ApJ, 502, L149

[1]*School of Physics, O'Brien Centre for Science North, University College Dublin, Belfield, Dublin 4, Ireland*
[2]*The Oskar Klein Centre, Department of Physics, AlbaNova, Stockholm University, SE-10691 Stockholm, Sweden*
[3]*INAF–Osservatorio Astronomico di Padova, Vicolo dell'Osservatorio 5, I-35122 Padova, Italy*
[4]*Department of Physics and Astronomy, University of Turku, FI-20014 Turku, Finland*
[5]*The Department of Physics, The University of Auckland, Private Bag 92019, Auckland, New Zealand*
[6]*The Oskar Klein Centre, Department of Astronomy, AlbaNova, Stockholm University, SE-10691 Stockholm, Sweden*
[7]*Max-Planck-Institut für Extraterrestrische Physik, Giessenbachstraße 1, D-85748 Garching, Germany*
[8]*Department of Astronomy, The Ohio State University, 140 W. 18th Avenue, Columbus, OH 43210, USA*
[9]*Center for Cosmology and AstroParticle Physics (CCAPP), The Ohio State University, 191 W. Woodruff Avenue, Columbus, OH 43210, USA*
[10]*Department of Physics and Astronomy, Texas A&M University, 4242 TAMU, College Station, TX 77843, USA*
[11]*Cerro Tololo Inter-American Observatory, NSF's National Optical-Infrared Astronomy Research Laboratory, Casilla 603, La Serena, Chile*
[12]*Institut d'Astrophysique de Paris (IAP), CNRS & Sorbonne Universite, 75014 Paris, France*
[13]*Kavli Institute for Astronomy and Astrophysics, Peking University, Yi He Yuan Road 5, Hai Dian District, Beijing 100871, China*
[14]*Institute of Space Sciences (ICE, CSIC), Campus UAB, Carrer de Can Magrans s/n, E-08193 Barcelona, Spain*
[15]*Steward Observatory, University of Arizona, 933 North Cherry Avenue, Tucson, AZ 85721-0065, USA*
[16]*Department of Physics, Florida State University, 77 Chieftan Way, Tallahassee, FL 32306, USA*
[17]*Tuorla Observatory, Department of Physics and Astronomy, University of Turku, FI-20014 Turku, Finland*
[18]*Finnish Centre for Astronomy with ESO (FINCA), University of Turku, FI-20014 Turku, Finland*
[19]*CBA–Kleinkaroo, Klein Karoo Observatory, PO Box 281, Calitzdorp 6660, South Africa*
[20]*Departamento de Ciencias Físicas, Universidad Andres Bello, Avda. Republica 252, Santiago 8320000, Chile*
[21]*Millennium Institute of Astrophysics, Camino El Observatorio 1515, Las Condes, Casilla, Santiago, Chile*
[22]*Department of Astronomy/Steward Observatory, 933 North Cherry Avenue, Rm N204, Tucson, AZ 85721-0065, USA*
[23]*Institute for Astronomy, University of Hawai'i, 2680 Woodlawn Drive, Honolulu, HI 96822, USA*
[24]*Astrophysics Research Centre, School of Maths and Physics, Queen's University Belfast, Belfast BT7 1NN, UK*
[25]*Mt Stromlo Observatory, The Research School of Astronomy and Astrophysics, Australian National University, ACT 2601, Australia*
[26]*National Centre for the Public Awareness of Science, Australian National University, Canberra, ACT 2611, Australia*
[27]*The ARC Centre of Excellence for All-Sky Astrophysics in 3 Dimension (ASTRO 3D), Mount Stromlo Rd Stromlo, Australian Capital Territory 2611, Australia*
[28]*Astronomical Observatory, University of Warsaw, Al. Ujazdowskie 4, PL-00478 Warszawa, Poland*
[29]*Institute of Astronomy, Madingley Road, Cambridge CB3 0HA, UK*
[30]*Unidad Mixta Internacional Franco-Chilena de Astronomía, CNRS/INSU UMI 3386 and Instituto de Astrofísica, Pontificia Universidad Católica de Chile, Santiago, Chile*
[31]*Aix Marseille Univ, CNRS, CNES, LAM, 13013 Marseille, France*
[32]*RHEA Group for ESA, European Space Astronomy Centre (ESAC–ESA), 28692, Madrid, Spain*
[33]*Kavli Institute for Cosmology, Institute of Astronomy, Madingley Road, Cambridge CB3 0HA, UK*
[34]*Las Cumbres Observatory, 6740 Cortona Drive, Suite 102, Goleta, CA 93117-5575, USA*
[35]*Department of Physics, University of California, Santa Barbara, CA 93106-9530, USA*
[36]*Center for Astrophysics | Harvard & Smithsonian, 60 Garden Street, Cambridge, MA 02138-1516, USA*
[37]*The NSF AI Institute for Artificial Intelligence and Fundamental Interactions*
[38]*The Observatories of the Carnegie Institution for Science, 813 Santa Barbara St, Pasadena, CA 91101, USA*
[39]*School of Physics & Astronomy, Cardiff University, Queens Buildings, The Parade, Cardiff CF24 3AA, UK*
[40]*School of Physics and Astronomy, University of Southampton, Southampton, Hampshire SO17 1BJ, UK*
[41]*School of Physics, Trinity College Dublin, The University of Dublin, Dublin 2, Ireland*
[42]*Department of Physics, University of the Free State, PO Box 339, Bloemfontein 9300, South Africa*
[43]*Carnegie Observatories, Las Campanas Observatory, Colina El Pino, Casilla 601, Chile*
[44]*Birmingham Institute for Gravitational Wave Astronomy and School of Physics and Astronomy, University of Birmingham, Birmingham B15 2TT, UK*
[45]*Institute for Astronomy, University of Edinburgh, Royal Observatory, Blackford Hill, Edinburgh EH9 3HJ, UK*
[46]*Nucleo de Astronomia de la Facultad de Ingenieria y Ciencias, Universidad Diego Portales, Av. Ejército 441, Santiago, Chile*
[47]*Department of Physics and Astronomy, University of North Carolina at Chapel Hill Chapel Hill, NC 27599, USA*
[48]*Department of Physics, Florida State University, 77 Chieftain Way, Tallahassee, FL 32306-4350, USA*
[49]*Department of Physics and Astronomy, Aarhus University, Ny Munkegade, DK-8000 Aarhus C, Denmark*
[50]*Department of Physics, University of Warwick, Coventry CV4 7AL, UK*
[51]*Astrophysics Research Centre, School of Mathematics and Physics, Queen's University Belfast, Belfast BT7 1NN, UK*

This paper has been typeset from a TEX/LATEX file prepared by the author.

Downloaded from https://academic.oup.com/mnras/article/513/4/5666/6581584 by University of Arizona user on 02 September 2022